Available online at www.sciencedirect.com
ScienceDirect
Mathematics and Computers in Simulation 211 (2023) 301–328
MATHEMATICS AND COMPUTERS IN SIMULATION
www.elsevier.com/locate/matcom

Original articles

The virtual element method for a 2D incompressible MHD system

S. Naranjo-Alvarez[a,b], L. Beirão da Veiga[a,*], V.A. Bokil[b], F. Dassi[a], V. Gyrya[c], G. Manzini[c]

[a] *Dipartimento di Matematica e Applicazioni, Università degli Studi di Milano-Bicocca, Italy*
[b] *Department of Mathematics 368 Kidder Hall Oregon State University, Corvallis, OR 97330, USA*
[c] *T-5 Group, Theoretical Division, Los Alamos National Laboratory, NM 87545, USA*

Received 9 August 2022; received in revised form 10 March 2023; accepted 23 March 2023
Available online 14 April 2023

Abstract

We present a novel discretization for the two-dimensional incompressible Magnetohydrodynamics (MHD) system coupling an electromagnetic model and a fluid flow model. Our approach follows the framework of the Virtual Element Method and offers two main advantages. The method can be implemented on unstructured meshes making it highly versatile and capable of handling a broad set of problems involving interfaces, free-boundaries, or adaptive refinements of the mesh. The second advantage concerns the divergence of the magnetic flux field and the fluid velocity. Our approach guarantees that the numerical approximation of the magnetic flux field and the fluid velocity are divergence free if their initial states are divergence free. Importantly, the divergence-free condition for the fluid velocity is satisfied in a pointwise sense. We include a theoretical proof of the condition on the magnetic flux field, energy estimates and a well-posedness study. Numerical testing confirms robustness of the method and its convergence properties on a variety of meshes.

Keywords: Virtual element methods; Magneto-hydrodynamics; Computation; Simulation

1. Introduction

In the last few decades, the number of applications involving magnetized fluids has skyrocketed, and the scientific community has made significant efforts to develop many predictive mathematical models. Magnetohydrodynamics (MHD) is one approach that has stood the test of time and has become a standard. The MHD model, its derivation, and its properties are well understood; see, for example, [22,33]. MHD relies on the interaction of fluid flow and electromagnetics. Maxwell's equations describe how we model electromagnetics, whereas conservation principles, precisely momentum and mass conservation, describe fluid motion.

This study aims to develop a novel discretization for the two-dimensional MHD model using the Virtual Element Method (VEM) framework. The VEM evolved from the Mimetic Finite Difference Method (MFD), for which we refer to [16,27,42]. We recall that the MFD method's guiding philosophy is based on a discrete mimicry of vector and tensor calculus so that the model's essential properties have a discrete compatible counterpart. Faraday's Law from Maxwell's equation implies that the magnetic fields are solenoidal, i.e., their divergence is always zero.

* Corresponding author.
E-mail addresses: sebastian.naranjo@unimib.it (S. Naranjo-Alvarez), lourenco.beirao@unimib.it (L. Beirão da Veiga), bokilv@oregonstate.edu (V.A. Bokil), franco.dassi@unimib.it (F. Dassi), gyrya@lanl.gov (V. Gyrya), gmanzini@lanl.gov (G. Manzini).

https://doi.org/10.1016/j.matcom.2023.03.029

When discretizing the electromagnetics system, we must maintain this condition, see [14] for further information. In particular, discrete divergence-free magnetic fields are a major advantage. Since we mimic the continuous setting and such a setting meets the magnetic field divergence criterion, a VEM for MHD naturally provides solenoidal magnetic field approximations. This work aims to prove and validate this condition.

The mesh flexibility is the second significant advantage of the MFD approach inherited by the VEM. The MFD method and, consequently, the VEM work on unstructured polytopal meshes whose elements can have general, even nonconvex, geometrical shapes. A recent study on the VEM robustness on meshes with severe deformations is found in [37].

These features have determined so far the success of the VEM in a wide range of applications, see, for example, [3–5,9,11–13,17,18,24,44].

We build on [35] to design a VEM for an electromagnetic subsystem. We also model electromagnetics and fluid flow with the lowest-order VEM proposed in [10,38].

We define each virtual element approximation space on a given mesh element through the solutions of a local PDE problem. Such a numerical approach employs only the degrees of freedom, avoiding pointwise shape function computation. To do this, we introduce projectors onto polynomial spaces, the most crucial ones being the L^2-orthogonal projectors. In particular, the L^2 projector is computable in some approximation spaces through a general strategy called the enhancement process introduced in [2] and first applied to Maxwell's equations in [9,39,40].

Since the continuous model involves several non-linearities, we propose a linearization that stems from a linear extrapolation of the magnetic field. This strategy has been initially suggested in [25] for a FEM. Its main advantage is that we need to solve only one linear system at each time step. We further prove that this method is well-posed by studying each linear system. To this end, we identify each system as a saddle-point problem, and the well-posedness of the VEM follows from the more general BBL theory. The well-posedness guarantees the stability of our computations. Importantly, it may serve as a basis for coming up with efficient preconditioners, which will be the topic of our future research in this field.

This paper is structured as follows. In Section 2 we present the continuous and discrete models. In Section 3, we provide the formal definition of the virtual element approximation spaces and detail the scheme's construction. In Section 4, we present the energy estimates and provide evidence of the method's stability. In Section 5, we discuss the linearization strategy; we prove the well-posedness of the linear solver and we confirm that the approximate magnetic field is divergence-free. In Section 6 we prove the well-posedness of the method. In Section 7 we offer a set of numerical experiments, including a convergence test and a model of the well-known cavity benchmark problem. Finally, in Section 8 we summarize our findings and expose possible further work.

1.1. Notation and preliminary technicalities

Mesh regularity. The virtual element method is formulated on a family of mesh partitions of the computational domain Ω, here denoted by $\{\Omega_h\}_h$. Each mesh Ω_h is a collection of nonoverlapping, closed polygonal cells K with boundary ∂K, area $|K|$, and diameter h_K, such that $\overline{\Omega} = \cup_K K$, and is labeled by the mesh size parameter $h = \max_K h_K$. We denote each edge of ∂K by e and the edge length by $|e| = h_e$.

In the VEM formulation, we normally ask the mesh family $\{\Omega_h\}_h$ to satisfy a few regularity conditions. These regularity conditions are such that the standard approximation estimates (e.g., for the interpolation operator) and properties of the finite element method necessary for the convergence analysis extend to the VEM. We report these regularity conditions below as they also determine the kind of meshes that can be used by the VEM. Such meshes must be *regular* in the sense that the two following conditions hold for some non-negative real number ρ independent of h:

(M1) (*star-shapedness*): every polygonal cell K of every mesh Ω_h is star-shaped with respect to a disk of radius ρh_K;

(M2) (*uniform scaling*): every edge $e \in \partial K$ of cell $K \in \Omega_h$ satisfies $h_e \geq \rho h_K$.

These assumptions on the mesh regularity are not quite restrictive and allow us to use polygonal elements with very general geometric shapes, as for example nonconvex elements or elements with hanging nodes. It is worth

noting that the hypotheses above can even be further relaxed. A review recent of this topic can be found, for example, in [37].

Other important implications of **(M1)–(M2)** are:

(i) every polygonal element is *simply connected*;
(ii) the number of edges of each polygonal cell in the mesh family $\{\Omega_h\}_h$ is uniformly bounded;
(iii) a polygonal element cannot have *arbitrarily small* edges with respect to its diameter for $h \to 0$.

Sobolev spaces. According to [1], $L^2(D)$ denotes the Lebesgue space of real-valued square integrable functions defined on D; $L^2_0(D)$ is the subspace of the functions in $L^2(D)$ having zero average on D; for any integer number $s > 0$, $H^s(D)$ is the Sobolev space s of the real-valued functions in $L^2(D)$ with all weak partial derivatives of order up to s in $L^2(D)$; $\left[L^2(D)\right]^2$, $\left[L^2_0(D)\right]^2$, and $\left[H^s(D)\right]^2$ are the vector versions of these spaces.

We denote the inner product in $L^2(D)$ and $H^s(D)$ by $(v, w)_D$ and $(v, w)_{s,D}$, respectively; we also denote the corresponding induced norms by $\|v\|_D$ and $\|v\|_{s,D}$, and the seminorm in $H^s(D)$ by $|v|_{s,D}$. When D is the whole computational domain, i.e., $D = \Omega$, we prefer to omit the subindex Ω and rather use the notation (v, w), $\|v\|$, $\|v\|_s$, etc. instead of $(v, w)_\Omega$, $\|v\|_\Omega$, $\|v\|_{s,\Omega}$, etc.

In the light of these definitions, for a given $s > 0$, we introduce the functional spaces

$$H^s(\mathrm{div}, D) := \left\{\mathbf{v} \in \left[H^s(D)\right]^2 \mid \mathrm{div}\,\mathbf{v} \in H^s(D)\right\}, \tag{1}$$

$$H^s(\mathbf{rot}, D) := \left\{\mathbf{v} \in \left[H^s(D)\right]^2 \mid \mathbf{rot}\,\mathbf{v} \in \left[H^s(D)\right]^2\right\}. \tag{2}$$

If $s = 0$, we write $H(\mathrm{div}, D)$ and $H(\mathbf{rot}, D)$ instead of $H^0(\mathrm{div}, D)$ and $H^0(\mathbf{rot}, D)$, which corresponds to $\left[H^1(D)\right]^2$. Let $\mathbf{n}_D$ be the unit vector orthogonal to the boundary ∂D and pointing out of D. According, e.g., to [32, Section 3.5], for the spaces (1) and (2), we can define the trace operators γ_{div} and $\gamma_{\mathbf{rot}}$ for the vector-valued functions in $H(\mathrm{div}, D)$ and $H(\mathbf{rot}, D)$. These operators are such that

$$\gamma_{\mathrm{div}}(\mathbf{v}) := \mathbf{n}_D \cdot \mathbf{v}, \qquad \gamma_{\mathbf{rot}}(\mathbf{v}) := \mathbf{n}_D \times \mathbf{v}.$$

Using the trace operators, we define the subspaces of $H^s(\mathrm{div}, D)$ and $H^s(\mathbf{rot}, D)$ with zero trace on the boundary

$$H^s_0(\mathrm{div}, D) := \left\{\mathbf{v} \in H^s(\mathrm{div}, D) \mid \gamma_{\mathrm{div}}(\mathbf{v}) = 0\right\},$$
$$H^s_0(\mathbf{rot}, D) := \left\{\mathbf{v} \in H^s(\mathbf{rot}, D) \mid \gamma_{\mathbf{rot}}(\mathbf{v}) = 0\right\}.$$

We use these subspaces to incorporate the homogeneous boundary conditions.

Polynomial spaces and orthogonal projection operator. We denote the space of polynomials of degree $\ell = 0, 1$ defined on element K and edge e by $\mathbb{P}_\ell(K)$, and $\mathbb{P}_\ell(e)$, respectively. We set $\mathbb{P}_{-1}(K) = \mathbb{P}_{-1}(e) = \{0\}$. The space $\mathbb{P}_1(K)$ is the span of the *scaled monomials* defined as

$$m_0(\mathbf{x}) = 1,\ m_1(\mathbf{x}) = \frac{x - x_K}{h_K},\ m_2(\mathbf{x}) = \frac{y - y_K}{h_K}, \qquad \forall \mathbf{x} = (x, y)^T \in K.$$

The basis of $\mathbb{P}_1(e)$ is defined in a similar way. We let $\mathbb{P}_\ell(\Omega_h)$ denote the space of the piecewise discontinuous polynomials of degree $\ell = 0, 1$ that are globally defined on Ω and such that $q_{|K} \in \mathbb{P}_1(K)$ for all elements $K \in \Omega_h$.

In the forthcoming discrete formulation, for any element K in Ω_h, we will use polynomial projectors denoted either by $\Pi^{0,K}_\ell : L^2(K) \to \mathbb{P}_\ell(K)$ or $\widetilde{\Pi}^K_\ell : L^2(K) \to \mathbb{P}_\ell(K)$, depending on whether they are orthogonal, i.e., satisfying that:

$$\left((\Pi^{0,K}_\ell v - v), q\right)_K = 0 \quad \forall q \in \mathbb{P}_\ell(K). \tag{3}$$

or oblique, when we only require only that

$$\widetilde{\Pi}^K_\ell q = q, \quad \forall q \in \mathbb{P}_\ell(K). \tag{4}$$

With an abuse of notation, we extend these definitions in a component-wise way to the multidimensional projection operator $\boldsymbol{\Pi}^{0,K}_\ell : [L^2(K)]^2 \to [\mathbb{P}_\ell(K)]^2$. We also define the global projection operators $\Pi^0_\ell, \widetilde{\Pi}_\ell : L^2(\Omega) \to \mathbb{P}_\ell(\Omega_h)$ and $\boldsymbol{\Pi}^0_\ell : \left[L^2(\Omega)\right]^2 \to \left[\mathbb{P}_\ell(\Omega_h)\right]^2$ as the operators respectively satisfying $\left(\Pi^0_\ell v\right)_{|K} = \Pi^{0,K}_\ell\left(v_{|K}\right)$ and $\left(\widetilde{\Pi}_\ell v\right)_{|K} = \widetilde{\Pi}^K_\ell\left(v_{|K}\right)$ for any smooth enough scalar function v as well as $\left(\boldsymbol{\Pi}^0_\ell \mathbf{v}\right)_{|K} = \boldsymbol{\Pi}^{0,K}_\ell\left(\mathbf{v}_{|K}\right)$ for any smooth enough vector field $\mathbf{v}$, and for all mesh elements $K \in \Omega_h$.

For simplicity of notation, whenever $\ell = 0$, we may omit the subindex 0, so using $\Pi^0 v$ and $\boldsymbol{\Pi}^0 \mathbf{v}$ instead of $\Pi_0^0 v$ and $\Pi_0^0 \mathbf{v}$, respectively, to denote the constant projections of a scalar function v or a vector function $\mathbf{v}$.

Other orthogonal operators used in the formulation of the VEM will be introduced when needed in the paper.

2. Continuous and discrete formulations

In the MHD model, we describe the dynamics of an electrically conducting fluid using the velocity field $\mathbf{u}$, the pressure field p, the electric field E and the magnetic flux field $\mathbf{B}$. The following system of equations governs the time evolution of these unknowns

$$\mathbf{u}_t - R_e^{-1}\Delta\mathbf{u} - s j \times \mathbf{B} + \nabla p = \mathbf{f} \qquad \text{in } \Omega, \tag{5a}$$

$$\mathbf{B}_t + \mathbf{rot}\, E = \mathbf{0} \qquad \text{in } \Omega, \tag{5b}$$

$$j - R_m^{-1}\mathrm{rot}\mathbf{B} = 0 \qquad \text{in } \Omega, \tag{5c}$$

$$\mathrm{div}\,\mathbf{B} = 0 \qquad \text{in } \Omega, \tag{5d}$$

$$\mathrm{div}\,\mathbf{u} = 0 \qquad \text{in } \Omega. \tag{5e}$$

The subscript t of $\mathbf{u}_t$ and $\mathbf{B}_t$ denotes the differentiation in time; R_e and R_m are the viscous and magnetic Reynolds numbers; s is the Hartman number and plays the role of a coupling coefficient; j is the current density given by

$$j := E + \mathbf{u} \times \mathbf{B}. \tag{6}$$

The quantities $\mathbf{u} = (u_x, u_y)^T$ and $\mathbf{B} = (B_x, B_y)^T$ (in bold fonts) are vector-valued fields, while p, E and j are scalar functions. Consistently, we redefine the cross products in (5a) and (6) as follows:

$$j \times \mathbf{B} = j \begin{pmatrix} -B_y \\ B_x \end{pmatrix} \quad \text{and} \quad \mathbf{u} \times \mathbf{B} = u_x B_y - u_y B_x. \tag{7}$$

We complete the MHD model with the initial conditions for the velocity and the magnetic fields,

$$\mathbf{u}(\mathbf{x}, 0) = \mathbf{u}_0(\mathbf{x}), \qquad \mathbf{B}(\mathbf{x}, 0) = \mathbf{B}_0(\mathbf{x}), \qquad \text{for all } \mathbf{x} \in \Omega, \tag{8}$$

and the boundary conditions for the velocity and the electric fields,

$$\mathbf{u}(\mathbf{x}, t) = \mathbf{u}_b^\partial(\mathbf{x}), \qquad E(\mathbf{x}, t) = E_b^\partial(\mathbf{x}) \qquad \text{for all } \mathbf{x} \in \partial\Omega \quad \text{and } t \in [0, T]. \tag{9}$$

We assume that the initial solution fields $\mathbf{u}_0$ and $\mathbf{B}_0$ are divergence free, i.e., $\mathrm{div}\,\mathbf{u}_0 = 0$ and $\mathrm{div}\,\mathbf{B}_0 = 0$. To ease the exposition, we assume that the boundary conditions are time-independent. In order to maintain the consistency of the formulation, we need that the boundary conditions on the velocity field satisfy

$$\int_{\partial\Omega} \mathbf{u}_b^\partial(\mathbf{x}) \cdot \mathbf{n}\, d\ell = 0. \tag{10}$$

2.1. Weak formulation

In the weak formulation of (5), for almost every $t \in [0, T]$ we search for

$$\Big(\mathbf{u}(t),\, p(t),\, E(t),\, \mathbf{B}(t)\Big) \in \big[H^1(\Omega)\big]^2 \times L_0^2(\Omega) \times H(\mathbf{rot}, \Omega) \times H(\mathrm{div}, \Omega),$$

such that

$$(\mathbf{u}_t, \mathbf{v}) - (p, \mathrm{div}\,\mathbf{v}) + R_e^{-1}(\nabla\mathbf{u}, \nabla\mathbf{v}) + s(j, \mathbf{v} \times \mathbf{B}) = (\mathbf{f}, \mathbf{v}) \qquad \forall \mathbf{v} \in \big[H_0^1(\Omega)\big]^2, \tag{11a}$$

$$(\mathbf{B}_t, \mathbf{C}) + (\mathbf{rot}\, E, \mathbf{C}) = 0 \qquad \forall \mathbf{C} \in H(\mathrm{div}, \Omega), \tag{11b}$$

$$(j, F) - R_m^{-1}(\mathbf{B}, \mathbf{rot}\, F) = 0 \qquad \forall F \in H_0(\mathbf{rot}, \Omega), \tag{11c}$$

$$(\mathrm{div}\,\mathbf{u}, q) = 0 \qquad \forall q \in L_0^2(\Omega), \tag{11d}$$

and with $\mathbf{u}$ and $\mathbf{B}$ satisfying the initial conditions (8) and the Dirichlet-type boundary conditions (9). In (11) the bilinear forms (ξ, η) and $(\boldsymbol{\xi}, \boldsymbol{\eta})$ stand for the L^2 inner products

$$(\xi, \eta) := \int_\Omega \xi(\mathbf{x})\eta(\mathbf{x})\, d\mathbf{x} \qquad \text{and} \qquad (\boldsymbol{\xi}, \boldsymbol{\eta}) := \int_\Omega \boldsymbol{\xi}(\mathbf{x}) \cdot \boldsymbol{\eta}(\mathbf{x})\, d\mathbf{x}. \tag{12}$$

The divergence-free condition on $\mathbf{B}$, see (5d), is not explicitly specified in the weak form since it is a consequence of (11b) combined with a solenoidal initial magnetic field $\mathbf{B}_0$. For notation's convenience, we used the formula $(j \times \mathbf{B}) \cdot \mathbf{v} = -(\mathbf{v} \times \mathbf{B}) \cdot j$ to rewrite the term $(j \times \mathbf{B}, \mathbf{v})$ as $(j, \mathbf{v} \times \mathbf{B})$ in Eq. (11a).

2.2. Semi-discrete weak formulation

The conforming virtual element approximation of (11) requires a polygonal meshing of the computational domain Ω, which we denote as Ω_h, and a set of finite dimensional subspaces of the functional spaces $\left[H^1(\Omega)\right]^2$, $L^2_0(\Omega)$, $H(\mathbf{rot}, \Omega)$, and $H(\mathrm{div}, \Omega)$. Note that $H(\mathbf{rot}, \Omega)$ is equivalent to $\left[H^1(\Omega)\right]^2$ in our two-dimensional setting. We denote these subspaces as

$$\begin{aligned} &\mathbf{W}_h \subset \left[H^1(\Omega)\right]^2, \quad &&\mathbf{W}_{0,h} \subset \left[H^1_0(\Omega)\right]^2, \quad &&Q_h \subset L^2_0(\Omega), \\ &V_h^{\mathrm{node}} \subset H(\mathbf{rot}, \Omega), \quad &&V_{0,h}^{\mathrm{node}} \subset H_0(\mathbf{rot}, \Omega), \quad &&\mathbf{V}_h^{\mathrm{edge}} \subset H(\mathrm{div}, \Omega), \end{aligned}$$

with the obvious inclusions

$$\mathbf{W}_{0,h} \subset \mathbf{W}_h, \quad V_{0,h}^{\mathrm{node}} \subset V_h^{\mathrm{node}}. \tag{13}$$

We assume that the following approximations are computable

$$\forall \mathbf{u}_h, \mathbf{v}_h \in \mathbf{W}_h : \; m_h(\mathbf{u}_h, \mathbf{v}_h) \approx (\mathbf{u}_h, \mathbf{v}_h), \quad a_h(\mathbf{u}_h, \mathbf{v}_h) \approx (\nabla \mathbf{u}_h, \nabla \mathbf{v}_h), \tag{14a}$$

$$\forall q_h \in Q_h, \mathbf{v}_h \in \mathbf{W}_h : \; b(\mathbf{v}_h, q_h) = (\mathrm{div}\, \mathbf{v}_h, q_h), \tag{14b}$$

$$\forall \mathbf{B}_h, \mathbf{C}_h \in \mathbf{V}_h^{\mathrm{edge}} : \; \left[\mathbf{B}_h, \mathbf{C}_h\right]_{\mathrm{edge}} \approx (\mathbf{B}_h, \mathbf{C}_h), \tag{14c}$$

$$\forall E_h, F_h \in V_h^{\mathrm{node}} : \; \left[E_h, F_h\right]_{\mathrm{node}} \approx (E_h, F_h). \tag{14d}$$

The formal definitions of all these mathematical objects, including the functional spaces, and the discussion of their properties will be the topics of the next section. Using these definitions, we introduce the semi-discrete virtual element approximation of problem (11):

For almost every $t \in [0, T]$, *find* $\mathbf{u}_h(t) \in \mathbf{W}_h$, $p_h(t) \in Q_h$, $\mathbf{B}_h(t) \in \mathbf{V}_h^{\mathrm{edge}}$, $E_h(t) \in V_h^{\mathrm{node}}$, *such that:*

$$\begin{aligned} &m_h(\mathbf{u}_{h,t}, \mathbf{v}_h) + R_e^{-1} a_h(\mathbf{u}_h, \mathbf{v}_h) - b(\mathbf{v}_h, p_h) + s(\widetilde{\Pi} E_h, \Pi^0 \mathbf{v}_h \times \Pi^0 \mathbf{B}_h) \\ &\qquad + (\Pi^0 \mathbf{u}_h \times \Pi^0 \mathbf{B}_h, \Pi^0 \mathbf{v}_h \times \Pi^0 \mathbf{B}_h) = \left(\mathbf{f}_h, \mathbf{v}_h\right) \qquad \forall \mathbf{v}_h \in \mathbf{W}_{0,h}, \end{aligned} \tag{15a}$$

$$\begin{aligned} &\left[E_h, F_h\right]_{\mathrm{node}} + (\Pi^0 \mathbf{u}_h \times \Pi^0 \mathbf{B}_h, \Pi^0 F_h) \\ &\qquad - R_m^{-1} \left[\mathbf{B}_h, \mathbf{rot}\, F_h\right]_{\mathrm{edge}} = 0 \qquad \forall F_h \in V_{0,h}^{\mathrm{node}}, \end{aligned} \tag{15b}$$

$$\left[\mathbf{B}_{h,t}, \mathbf{C}_h\right]_{\mathrm{edge}} + \left[\mathbf{rot}\, E_h, \mathbf{C}_h\right]_{\mathrm{edge}} = 0 \qquad \forall \mathbf{C}_h \in \mathbf{V}_h^{\mathrm{edge}}, \tag{15c}$$

$$b(\mathbf{u}_h, q_h) = 0 \qquad \forall q_h \in Q_h, \tag{15d}$$

where $\mathbf{u}_h$ and $\mathbf{B}_h$ at $t = 0$ are given by a suitable approximation of $\mathbf{u}_0$ and $\mathbf{B}_0$, the initial conditions (8). To simplify the notation, we omitted the time variable t. In (15a), we used the definition of j from (6), so that

$$(j, \mathbf{v} \times \mathbf{B}) = (E + \mathbf{u} \times \mathbf{B}, \mathbf{v} \times \mathbf{B}) = (E, \mathbf{v} \times \mathbf{B}) + (\mathbf{u} \times \mathbf{B}, \mathbf{v} \times \mathbf{B}).$$

Also, if v denotes a generic scalar field, $\Pi^0 v$ is the L^2-orthogonal projection of v onto $\mathbb{P}_0(\Omega_h)$, the discontinuous space of piecewise constant polynomials defined on every $K \in \Omega_h$. The extension to the vector case, i.e., the polynomial projection $\Pi^0 \mathbf{v}$ of a generic vector valued-field $\mathbf{v}$, is straightforward in the component-wise sense. The formal definition of these projection operators will be given in (48).

2.3. Fully discrete virtual element formulation

Finally, we present the fully discrete virtual element approximation of problem (11). To this end, we split the time interval $[0, T]$ into N equally-sized subintervals with size $\Delta t > 0$, the timestep, so that $T = N \Delta t$. These subintervals form a collocated grid in time composed of the $(N+1)$ points $\left\{t^n = n\Delta t\right\}_{n=0}^{N}$. We evaluate the unknown fields $\mathbf{u}_h$, p_h, E_h, and $\mathbf{B}_h$ at these discrete times, and denote such evaluations by the discrete quantities

$$\mathbf{u}_h^n \approx \mathbf{u}(n\Delta t), \quad \mathbf{B}_h^n \approx \mathbf{B}(n\Delta t), \quad E_h^n \approx E(n\Delta t), \quad p_h^n \approx p(n\Delta t), \tag{16}$$

indexed with a superscript n. For the sake of convenience we also define the discrete differential operator δ_{t^n} in time, so that

$$\forall n \in [1, N]: \quad \delta_t^n \mathbf{u}_h = \frac{\mathbf{u}_h^n - \mathbf{u}_h^{n-1}}{\Delta t}, \qquad \delta_t^n \mathbf{B}_h = \frac{\mathbf{B}_h^n - \mathbf{B}_h^{n-1}}{\Delta t}. \tag{17}$$

We define a "discrete" current density $j_h^n \approx j(\cdot, t^n)$ by

$$j_h^n := \widetilde{\Pi} E_h^n + \Pi^0 \mathbf{u}_h^n \times \Pi^0 \mathbf{B}_h^n. \tag{18}$$

The fully-discrete virtual element formulation of Eqs. (15) is obtained by applying the backward-Euler discretization in time and reads as:

For each $n \in [1, N]$, find $(\mathbf{u}_h^n, p_h^n, \mathbf{B}_h^n, E_h^n) \in \mathbf{W}_h \times Q_h \times \mathbf{V}_h^{\text{edge}} \times V_h^{\text{node}}$, such that:

$$\begin{aligned}
&m_h(\delta_t^n \mathbf{u}_h, \mathbf{v}_h) + R_e^{-1} a_h(\mathbf{u}_h^n, \mathbf{v}_h) - b(\mathbf{v}_h, p_h^n) \\
&\qquad + s(j_h^n, \Pi^0 \mathbf{v}_h \times \Pi^0 \mathbf{B}_h^n) = \left(\mathbf{f}_h^n, \mathbf{v}_h\right) \qquad \forall \mathbf{v}_h \in \mathbf{W}_{0,h}, && \text{(19a)} \\
&\left[E_h^n, F_h\right]_{\text{node}} + (\Pi^0 \mathbf{u}_h^n \times \Pi^0 \mathbf{B}_h^n, \Pi^0 F_h) \\
&\qquad - R_m^{-1} \left[\mathbf{B}_h^n, \mathbf{rot}\, F_h\right]_{\text{edge}} = 0 \qquad \forall F_h \in V_{0,h}^{\text{node}}, && \text{(19b)} \\
&\left[\delta_t^n \mathbf{B}_h, \mathbf{C}_h\right]_{\text{edge}} + \left[\mathbf{rot}\, \mathbf{E}_h^n, \mathbf{C}_h\right]_{\text{edge}} = 0 \qquad \forall \mathbf{C}_h \in \mathbf{V}_h^{\text{edge}}, && \text{(19c)} \\
&b(\mathbf{u}_h^n, q_h) = 0 \qquad \forall q_h \in Q_h. && \text{(19d)}
\end{aligned}$$

As is done for system (15), we set the initial states $\mathbf{B}^0$ and $\mathbf{u}^0$ through a divergence-free approximation of $\mathbf{B}_0$ and $\mathbf{u}_0$.

We note that in the above formulation the boundary conditions are implicit in the definition of the discrete spaces $\mathbf{W}_h$ and V_h^{node}, which include a discrete version of (9). In practice, we extend the boundary conditions E_b and $\mathbf{u}_b$ to the interior of Ω, then we embed them into the their respective discrete spaces using suitable interpolation operators $\mathfrak{I}(\mathbf{u}_b) \in \mathbf{W}_h$ and $\mathcal{I}_{\text{node}}(E_b) \in V_h^{\text{node}}$ (which will be described in detail later on). At each time step we look for $\hat{\mathbf{u}}_h \in \mathbf{W}_{0,h}$ and $\hat{E}_h \in V_{0,h}^{\text{node}}$ such that:

$$\mathbf{u}_h^n = \mathfrak{I}(\mathbf{u}_b) + \hat{\mathbf{u}}_h, \quad E_h^n = \mathcal{I}_{\text{node}}(E_b) + \hat{E}_h. \tag{20}$$

3. Virtual element method

3.1. VEM for Navier–Stokes equations

The conforming virtual element space used in the discretization of the fluid-flow equations in (19) was originally proposed in [7,8,38]. Here, we consider the enhanced formulation introduced in [38]. This formulation allows us to compute the L^2-orthogonal projection onto the largest polynomial subspace contained in the space of shape functions. Such operator is used in the construction of the approximate mass matrices.

First, we focus on the construction of the space for the velocity approximation. We consider a cell $K \in \Omega_h$ and the auxiliary spaces:

- $\mathbb{B}_2(\partial K) := \left\{ v \in C^0(\partial K): \ v_{|e} \in \mathbb{P}_2(e), \ \forall e \in \partial K \right\}$;
- $\mathcal{G}_2(K) := \nabla \mathbb{P}_3(K) \subset \left[\mathbb{P}_2(K)\right]^2$;
- $\mathcal{G}_2^{\oplus}(K) := \mathbf{x}^{\oplus} \mathbb{P}_1(K) \subset \left[\mathbb{P}_2(K)\right]^2$, with $\mathbf{x}^{\oplus} = (x_2, -x_1)^T$, so that the following direct sum decomposition holds: $\left[\mathbb{P}_2(K)\right]^2 = \mathcal{G}_2(K) \oplus \mathcal{G}_2^{\oplus}(K)$.

According to [8,38], we introduce a set of bounded linear functionals, which associate every vector-valued field $\mathbf{v}_h \in \mathbf{W}_h(K)$ with:

- **(Dv1)**: the values of $\mathbf{v}_h$ at the vertices of element K;
- **(Dv2)**: the values of $\mathbf{v}_h$ at the midpoint of every edge $e \in \partial K$;
- **(Dv3)**: the integral moment of $\mathbf{v}_h$ over K against $\mathbf{g}_0^{\oplus} = \mathbf{x}^{\oplus} \in \mathcal{G}_1^{\oplus}(K)$:

$$\frac{1}{|K|} \int_K \mathbf{v}_h \cdot \mathbf{x}^{\oplus} \, d\mathbf{x}.$$

- **(Dv4)**: the integral moments of $\operatorname{div}\mathbf{v}_h$ over K against a basis for $\mathbb{P}_1(K)/\mathbb{R}$:

$$\int_K \operatorname{div}\mathbf{v}_h \frac{x - x_K}{h_K}\ d\mathbf{x}, \quad \text{and} \quad \int_K \operatorname{div}\mathbf{v}_h \frac{y - y_K}{h_K}\ d\mathbf{x}.$$

Let the elliptic projection operator $\boldsymbol{\Pi}_2^{\nabla,K} : \left[H^{s+1}(K)\right]^2 \to \left[\mathbb{P}_2(K)\right]^2$, $s > 0$, be defined such that for every $\mathbf{v}_h \in \mathbf{V}_h(K)$, the vector polynomial $\boldsymbol{\Pi}_2^{\nabla,K}\mathbf{v}_h$ is the unique solution to the variational problem:

$$\int_K \nabla\mathbf{q} : \nabla\left(\mathcal{I} - \boldsymbol{\Pi}_2^{\nabla,K}\right)\mathbf{v}_h\ d\mathbf{x} = 0 \qquad \forall\mathbf{q} \in \left[\mathbb{P}_2(K)\right]^2,$$
$$\boldsymbol{\Pi}_0^{0,K}\left(\mathcal{I} - \boldsymbol{\Pi}_2^{\nabla,K}\right)\mathbf{v}_h = \mathbf{0},$$

where $\mathcal{I}$ is the identity operator. Since the vector polynomial $\boldsymbol{\Pi}_2^{\nabla,K}\mathbf{v}_h$ is computable by using only the values **(Dv1)–(Dv4)** of $\mathbf{v}_h$, we use it to define the virtual element space for the velocity approximation:

$$\mathbf{W}_h(K) := \left\{\mathbf{v}_h \in \mathbf{U}_h(K) :\ \left(\left(\mathcal{I} - \boldsymbol{\Pi}_2^{\nabla,K}\right)\mathbf{v}_h, \mathbf{g}^{\oplus}\right)_K = 0\ \ \forall\mathbf{g}^{\oplus} \in \mathcal{G}_2^{\oplus}(K) \setminus \mathcal{G}_0^{\oplus}(K)\right\}, \tag{21}$$

where $\mathcal{G}_2^{\oplus}(K)\setminus\mathcal{G}_0^{\oplus}(K)$ is the subspace of polynomials in $\mathcal{G}_2^{\oplus}(K)$ that are L^2-orthogonal to all polynomials in $\mathcal{G}_0^{\oplus}(K)$, and

$$\mathbf{U}_h(K) := \Big\{\mathbf{v}_h \in \left[H^1(K)\right]^2 : \mathbf{v}_{h|\partial K} \in \left[\mathbb{B}_2(\partial K)\right]^2,\ \operatorname{div}\mathbf{v}_h \in \mathbb{P}_1(K),$$
$$-\Delta\mathbf{v}_h - \nabla s \in \mathcal{G}_2^{\oplus}(K) \quad \text{for some } s \in L_0^2(K)\Big\}. \tag{22}$$

All operators and equations in the previous definitions must be interpreted in the distributional sense.

The set of values provided by **(Dv1)–(Dv4)** is unisolvent in $\mathbf{W}_h(K)$ and we can take these functionals as the degrees of freedom of the space. Importantly, we can compute all the moments of $\mathbf{v}_h \in \mathbf{W}_h(K)$ against the vector polynomials of degrees up to 2, i.e., all integrals like

$$\int_K \mathbf{v}_h \cdot \mathbf{q} \qquad \forall\mathbf{q} \in \left[\mathbb{P}_2(K)\right]^2,$$

using only the values from **(Dv1)–(Dv4)** of $\mathbf{v}_h$. This fact follows on decomposing $\mathbf{q} = \nabla q_3 + \mathbf{g}_2^{\oplus}$, where $q_3 \in \mathbb{P}_3(K)$ and $\mathcal{G}_2^{\oplus}(K)$, integrating by part the term containing ∇q_3 and noting that the divergence of $\mathbf{v}_h$ is computable from **(Dv1)–(Dv2)** and **(Dv4)**, while the term containing $\mathbf{g}_2^{\oplus}$ comes from **(Dv3)**. Thus, the orthogonal projection operator $\boldsymbol{\Pi}_2^{0,K} : \mathbf{W}_h(K) \to \left[\mathbb{P}_2(K)\right]^2$, which is defined as

$$\int_K \mathbf{q} \cdot \left(\mathcal{I} - \boldsymbol{\Pi}_2^{0,K}\right)\mathbf{v}_h\ d\mathbf{x} = 0 \qquad \forall\mathbf{q} \in \left[\mathbb{P}_2(K)\right]^2,$$

is computable in $\mathbf{W}_h(K)$. Then, the global velocity space is

$$\mathbf{W}_h := \left\{\mathbf{v}_h \in \left[H^1(\Omega)\right]^2 : \forall K \in \Omega_h,\ \mathbf{v}_{h|K} \in \mathbf{W}_h(K)\ \forall K \in \Omega_h\right\}.$$

In the virtual element approximation of the momentum equation, we use the bilinear forms

$$a_h(\mathbf{u}_h, \mathbf{v}_h) = \sum_{K\in\Omega_h} a_h^K(\mathbf{u}_h, \mathbf{v}_h), \tag{23}$$

where

$$a_h^K(\mathbf{u}_h, \mathbf{v}_h) = \left(\nabla\boldsymbol{\Pi}_2^{\nabla,K}\mathbf{u}_h, \nabla\boldsymbol{\Pi}_2^{\nabla,K}\mathbf{v}_h\right)_K + \mathcal{S}_h^K\left((\mathcal{I} - \boldsymbol{\Pi}_2^{\nabla,K})\mathbf{u}_h, (\mathcal{I} - \boldsymbol{\Pi}_2^{\nabla,K})\mathbf{v}_h\right). \tag{24}$$

and

$$m_h(\mathbf{u}_h, \mathbf{v}_h) = \sum_{K\in\Omega_h} m_h^K(\mathbf{u}_h, \mathbf{v}_h), \tag{25}$$

where

$$m_h^K(\mathbf{u}_h, \mathbf{v}_h) = (\boldsymbol{\Pi}_2^{0,K}\mathbf{u}_h, \boldsymbol{\Pi}_2^{0,K}\mathbf{v}_h)_K + |K|\mathcal{S}_h^K\left((\mathcal{I} - \boldsymbol{\Pi}_2^{0,K})\mathbf{u}_h, (\mathcal{I} - \boldsymbol{\Pi}_2^{0,K})\mathbf{v}_h\right), \tag{26}$$

which are defined for all pairs of vector-valued functions $\mathbf{u}_h, \mathbf{v}_h \in \mathbf{W}_h$. In (24) and (26), the bilinear form $\mathcal{S}_h^K(\cdot,\cdot)$ is a suitable stabilization term, see [38].

The bilinear forms (24) and (26) satisfy the stability and consistency properties

- **Stability**: there exist two pairs of real positive constants (μ_*, μ^*) and (α_*, α^*) independent of h (and K) such that

$$\alpha_* \|\mathbf{v}_h\|_{1,K}^2 \leq \ a_h^K(\mathbf{v}_h, \mathbf{v}_h) \leq \alpha^* \|\mathbf{v}_h\|_{1,K}^2 \qquad \forall \mathbf{v}_h \in \mathbf{W}_h(K)^2. \tag{27}$$

and

$$\mu_* \|\mathbf{v}_h\|_{0,K}^2 \leq m_h^K(\mathbf{v}_h, \mathbf{v}_h) \leq \ \mu^* \|\mathbf{v}_h\|_{0,K}^2 \qquad \forall \mathbf{v}_h \in \mathbf{W}_h(K)^2, \tag{28}$$

- **Consistency**:

$$a_h^K(\mathbf{v}_h, \mathbf{q}) = a^K(\mathbf{v}_h, \mathbf{q})_K \qquad \forall \mathbf{v}_h \in \mathbf{W}_h(K), \ \ \mathbf{q} \in \left[\mathbb{P}_2(K)\right]^2. \tag{29}$$

and

$$m_h^K(\mathbf{v}_h, \mathbf{q}) = (\mathbf{v}_h, \mathbf{q})_K \qquad \forall \mathbf{u}_h \in \mathbf{W}_h(K), \ \ q \in \mathbb{P}_2(K), \tag{30}$$

Now, we introduce the pressure space. We define the local space of pressures over cell K as $Q_h^*(K) := \mathbb{P}_1(K)$. Every function $q \in Q_h^*(K)$ is uniquely described by the following set of degrees of freedom, which are the elemental moment against the linear polynomials

$$\frac{1}{|K|}\int_K \frac{x - x_K}{h_K} q \, d\mathbf{x}, \qquad \frac{1}{|K|}\int_K \frac{y - y_K}{h_K} q \, d\mathbf{x}, \qquad \text{and} \qquad \frac{1}{|K|}\int_K q \, d\mathbf{x}.$$

We define the global pressure space as

$$Q_h^* = \left\{ q_h \in L^2(\Omega) : \forall K \in \Omega_h, \quad q_{h|K} \in Q_h^*(K) \right\}, \tag{31}$$

endowed with the inner product

$$\forall p_h, q_h \in Q_h^* : \quad b_h(p_h, q_h) = \sum_{K \in \Omega_h} b_h^K(p_h, q_h) \quad \text{for} \quad b_h^K(p_h, q_h) = \int_K p_h q_h \, d\mathbf{x}. \tag{32}$$

Finally, in formulation (19) we use

$$Q_h = \left\{ q_h \in Q_h^* : \ \int_\Omega q_h \, d\mathbf{x} = 0 \right\}. \tag{33}$$

The finite dimensional spaces $\mathbf{W}_h$ and Q_h are a stable Stokes pair, as stated in the following Theorem.

Theorem 3.1. *The spaces $\mathbf{W}_h$ and Q_h satisfy the inf–sup condition*

$$\inf_{q_h \in Q_h} \sup_{\mathbf{v}_h \in \mathbf{W}_h \setminus \{\mathbf{0}\}} \frac{(\operatorname{div} \mathbf{v}_h, q_h)}{\|\mathbf{v}_h\|_{\mathbf{V}_h} \|q\|_{Q_h}} \geq \beta > 0,$$

for some strictly positive, real constant β, where

$$\|\mathbf{v}_h\|_{\mathbf{V}_h} = (m_h(\mathbf{v}_h, \mathbf{v}_h) + a_h(\mathbf{v}_h, \mathbf{v}_h))^{1/2} \quad \text{and} \qquad \|q_h\|_{Q_h} = \left(\int_K |q_h|^2 \, d\mathbf{x} \right)^{1/2}.$$

Proof. See [8,38]. □

Definition 3.1. The interpolation operator $\mathfrak{I} : \left[H^{s+1}(\Omega)\right]^2 \to \mathbf{W}_h$, $s > 0$, is defined as follows. Given $\mathbf{v} \in \left[H^{s+1}(\Omega)\right]^2$, the function $\mathfrak{I}\mathbf{v}$ satisfies (**Dv1**)$\mathfrak{I}\mathbf{v} =$ (**Dv1**)$\mathbf{v}$ and the same holds for (**Dv3**) and (**Dv4**). Instead, the DoFs (**Dv2**) (i.e. the midpoint evaluations of $\mathfrak{I}(\mathbf{v})$) are selected so that such operator preserves the flux across all edges e of element K

$$\int_e \mathfrak{I}(\mathbf{v}) \cdot \mathbf{n} \, d\ell = \int_e \mathbf{v} \cdot \mathbf{n} \, d\ell. \tag{34}$$

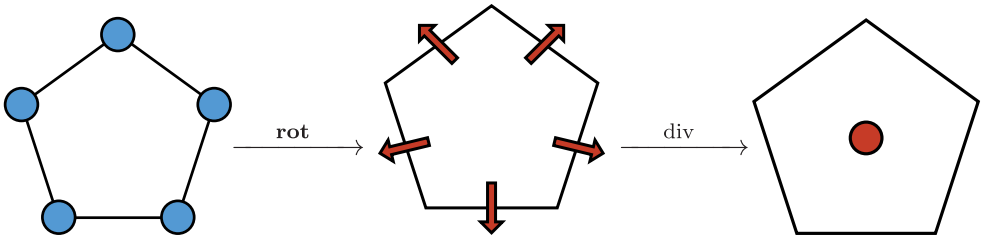

Fig. 1. Degrees of freedom of the virtual element spaces $V_h^{\text{node}}(K)$ defined in (38) (left panel), $\mathbf{V}_h^{\text{edge}}(K)$ defined in (47) (central panel), and $V_h^{\text{cell}}(K)$ defined in (56) (right panel). These three functional spaces and the differential operators **rot** and div form a de Rham chain. (For interpretation of the references to color in this figure legend, the reader is referred to the web version of this article.)

We define operator $\mathfrak{I}(\mathbf{v})$ in this way to have the following property on $b_h(\cdot,\cdot)$.

Lemma 3.2. *For any* $\mathbf{v} \in \left[H^{s+1}(\Omega)\right]^2$, $s > 0$, *and any* $p \in \mathbb{P}_1(\Omega_h)$, *the interpolation operator* $\mathfrak{I} : \left[H^{s+1}(\Omega)\right]^2 \to \mathbf{W}_{0,h}$ *locally preserves the bilinear form* $b_h(\cdot,\cdot)$ *in the sense that*

$$b_h^K(\mathfrak{I}\mathbf{v},\, p) = b_h^K(\mathbf{v},\, p) \qquad \forall K \in \Omega_h. \tag{35}$$

Proof. Consider a mesh element $K \in \Omega_h$ and a scalar function $p \in \mathbb{P}_1(K) \setminus \mathbb{R}$. Eq. (35) holds because operator $\mathfrak{I}$ preserves the degrees of freedom (**Dv4**). To prove that Eq. (35) also holds for constant fields, we test $\operatorname{div}(\mathfrak{I}\mathbf{v})$ against $p = 1$, integrate by parts and use (34). We find that

$$\begin{aligned} b_h^K(\mathfrak{I}\mathbf{v},\, 1) &= \int_K \operatorname{div}(\mathfrak{I}\mathbf{v})\, d\mathbf{x} = \sum_{e\in\partial K} \int_e \mathfrak{I}\mathbf{v}\cdot\mathbf{n}\, d\ell = \sum_{e\in\partial K} \int_e \mathbf{v}\cdot\mathbf{n}\, d\ell \\ &= \int_K \operatorname{div}(\mathbf{v})\ d\mathbf{x} = b_h^K(\mathbf{v},\, 1). \end{aligned} \tag{36}$$

This completes the proof due to linearity of $b_h^K(\cdot,\cdot)$. □

We conclude this subsection by defining the norm on the space of continuous linear operators that act on $\mathbf{W}_h$ by

$$|||\mathbf{f}_h|||_{-1,\mathbf{W}_h} := \inf_{\mathbf{v}_h\in\mathbf{W}_{0,h}} \frac{(\mathbf{f}_h,\, \mathbf{v}_h)}{a_h(\mathbf{v}_h,\, \mathbf{v}_h)}. \tag{37}$$

3.2. VEM for electromagnetic equations

The nodal space. Let $K \in \Omega_h$. The formal definition of the nodal elemental space is given by

$$\begin{aligned} V_h^{\text{node}}(K) := \Big\{\ & D_h \in H(\mathbf{rot}, K) : D_{h|\partial K} \in C^0(\partial K),\ D_{h|e} \in \mathbb{P}_1(e)\ \forall e \in \partial K, \\ & \operatorname{rot}\mathbf{rot}\, D_h = 0 \ \text{ in } K\ \Big\}. \end{aligned} \tag{38}$$

Every function $D_h \in V_h^{\text{node}}(K)$ is uniquely determined by

(V) the values $D_h(V)$ at the vertices V of cell K.

The set of the vertex values associated with element K is unisolvent in the elemental space $V_h^{\text{node}}(K)$ defined in (38). Accordingly, every set of vertex values uniquely defines a virtual element function in $V_h^{\text{node}}(K)$ and every function in $V_h^{\text{node}}(K)$ corresponds to a unique set of vertex values. Fig. 1 (left panel) shows the vertex values associated with a given cell K of the mesh as blue disks.

In the space $V_h^{\text{node}}(K)$ the orthogonal projection onto $\mathbb{P}_1$ is *non*-computable. The classical technique implemented in this situation is to enhance the space into another where such a projection is computable. Instead, we take a different approach. Here, we will define an oblique projection which we will denote $\widetilde{\Pi}^K$ satisfying:

P1 The projection $\widetilde{\Pi}^K D_h$ is computable from the degrees of freedom of D_h.
P2 If $D_h \in \mathbb{P}_1(K)$ then $\widetilde{\Pi}^K D_h = D_h$.
P3 There exists a constant $C > 0$ independent of mesh-size and time-step such that

$$\|\widetilde{\Pi}^K D_h\|_{0,K} \leq C\|D_h\|_{0,K}. \tag{39}$$

This, approach is original to [35] where the authors present three possible options. In the numerical results Section 7 we use the well-known elliptic projector. For $D_h \in V_h^{\text{node}}(K)$ the elliptic projector is the solution to the variational problem

$$\forall q \in \mathbb{P}_1(K): \quad \int_K \mathbf{rot}\left(D_h - \widetilde{\Pi}^K D_h\right) \cdot \mathbf{rot}\, q\, dA = 0, \tag{40a}$$

$$P_0(D_h - \widetilde{\Pi}^K D_h) = 0, \tag{40b}$$

where,

$$P_0(D_h) = \sum_V D_h(V). \tag{41}$$

We also define a global oblique projection operator $\widetilde{\Pi}: V_h^{\text{node}} \to \mathbb{P}_1(\Omega_h)$, that is such that $\widetilde{\Pi} D_{h|K} = \widetilde{\Pi}^K(D_{h|K})$ for all $K \in \Omega_h$, where $\mathbb{P}_1(\Omega_h)$ is the space of piecewise linear polynomials on mesh Ω_h.

On all element K, we define the local bilinear form

$$\left[E_h, D_h\right]_{\text{node},K} = \left(\widetilde{\Pi}^K E_h, \widetilde{\Pi}^K D_h\right)_K + \mathcal{S}^V\left(\left(1 - \widetilde{\Pi}^K\right)E_h, \left(1 - \widetilde{\Pi}^K\right)D_h\right), \tag{42}$$

where $\mathcal{S}^V$ is a suitable stabilization. In the VEM construction, for the stabilization $\mathcal{S}^V$ we usually consider *any* bilinear form for which there exist two real constants s_* and s^* independent of h such that

$$s_*\|D_h\|_{0,K}^2 \leq \mathcal{S}^V(D_h, D_h) \leq s^*\|D_h\|_{0,K}^2 \quad \forall D_h \in \ker \widetilde{\Pi}^K \cap V_h^{\text{node}}(K). \tag{43}$$

Practical choices for the stabilizations and the related analysis can be found in [15,43]. Since (42) defines an inner product on the elemental space $V_h^{\text{node}}(K)$, it induces the mesh-dependent norm $|||D_h|||_{\text{node},K} = \left[D_h, D_h\right]^{\frac{1}{2}}_{\text{node},K}$. The inner product (42) is stable and linearly consistent according to the following definitions:

- **Stability**: There exist two real constants α_* and $\alpha^* > 0$ independent of h (and K) such that

$$\alpha_*\|D_h\|_{0,K} \leq |||D_h|||_{V_h^{\text{node}}(K)} \leq \alpha^*\|D_h\|_{0,K} \quad \forall D_h \in V_h^{\text{node}}(K)^2. \tag{44}$$

- **Consistency**:

$$\left[D_h, q\right]_{\text{node},K} = \left(D_h, q\right)_K \quad \forall D_h \in V_h^{\text{node}}(K),\ q \in \mathbb{P}_1(K). \tag{45}$$

Finally, we define the global nodal space V_h^{node} by collecting together in the conforming way all the elemental virtual element spaces

$$V_h^{\text{node}} := \left\{D_h \in H(\mathbf{rot}, \Omega) : D_{h|K} \in V_h^{\text{node}}(K), \quad \forall K \in \Omega_h\right\}. \tag{46}$$

The functions in V_h^{node} are uniquely characterized by their nodal values at the mesh vertices, and their global unisolvence is a consequence of their unisolvence at the elemental level. Thus, we define $\mathcal{I}_{\text{node}}: C^\infty(\Omega) \to V_h^{\text{node}}$ such that $\mathcal{I}^{\text{node}}(D)$ and D share the same nodal evaluations. The global space V_h^{node} is endowed with the global inner product

$$\left[E_h, D_h\right]_{\text{node}} := \sum_{K \in \Omega_h} \left[E_h, D_h\right]_{\text{node},K}$$

and is an Hilbert space with induced norm $|||D_h|||_{\text{node}} = [D_h, D_h]^{\frac{1}{2}}$.

The edge space. The edge space that was introduced in [10] is the finite dimensional counterpart of $H(\mathrm{div}, \Omega)$. Its formal definition over the cell K reads as

$$\mathbf{V}_h^{\mathrm{edge}}(K) := \Big\{ \mathbf{C}_h \in H(\mathrm{div}, K) \cap H(\mathbf{rot}, K) : \mathrm{div}\, \mathbf{C}_h \in \mathbb{P}_0(K), \quad \mathrm{rot}\, \mathbf{C}_h = 0, \\ \mathbf{C}_{h|e} \cdot \mathbf{n} \in \mathbb{P}_0(e)\ \forall e \in \partial K \Big\}. \tag{47}$$

Every virtual element vector-valued field $\mathbf{C}_h \in \mathbf{V}_h^{\mathrm{edge}}(K)$ is characterized by

(E) the moment of its flux across all the elemental edges

$$\forall e \in \partial K : \quad \frac{1}{|e|} \int_e \mathbf{C}_h \cdot \mathbf{n} d\ell.$$

The set of values associated with the edges of the boundary of a given element K is unisolvent in the elemental space $\mathbf{V}_h^{\mathrm{edge}}(K)$ defined in (47). Fig. 1 (central panel) shows such values as red arrows pointing out of element K.

An important property of space $\mathbf{V}_h^{\mathrm{edge}}(K)$ is that the orthogonal projection $\Pi^{0,K} : \mathbf{V}_h^{\mathrm{edge}}(K) \to \mathbb{P}_0(K)$ is computable using the degrees of freedom **(E)**. This operator is such that for every $\mathbf{C}_h \in \mathbf{V}_h^{\mathrm{edge}}(K)$, the constant polynomial $\Pi^{0,K}_{\mathbf{C}_h}$ is the solution to the variational problem

$$\big(\mathbf{C}_h - \Pi^{0,K}\mathbf{C}_h, \mathbf{q}\big)_K = 0 \qquad \forall \mathbf{q} \in \big[\mathbb{P}_0(K)\big]^2. \tag{48}$$

We define the inner product in the space $\mathbf{V}_h^{\mathrm{edge}}(K)$ by using the projection operator $\Pi^{0,K}$, so that

$$\big[\mathbf{B}_h, \mathbf{C}_h\big]_{\mathrm{edge},K} = \big(\Pi^{0,K}\mathbf{B}_h, \Pi^{0,K}\mathbf{C}_h\big)_K + \mathcal{S}^e\big((\mathcal{I} - \Pi^{0,K})\mathbf{B}_h, (\mathcal{I} - \Pi^{0,K})\mathbf{C}_h\big) \tag{49}$$

for every possible pair of virtual element functions $\mathbf{B}_h$, $\mathbf{C}_h \in \mathbf{V}_h^{\mathrm{edge}}(K)$. As before, we need a stabilization term, e.g., $\mathcal{S}^e$, which can be *any* continuous bilinear form for which there exist two strictly positive constants s_* and s^* independent of h such that

$$s_* \|\mathbf{C}_h\|^2_{0,K} \le \mathcal{S}^e(\mathbf{C}_h, \mathbf{C}_h) \le s^* \|\mathbf{C}_h\|^2_{0,K} \quad \forall \mathbf{C}_h \in \ker \Pi^{0,K} \cap \mathbf{V}_h^{\mathrm{edge}}(K), \tag{50}$$

(the two constants s_* and s^* are not the same of Eq. (43)). Practical choices of the stabilization term $\mathcal{S}^e(\cdot,\cdot)$ can be found in [10]. This inner product induces the norm

$$|||\mathbf{C}_h|||_{\mathrm{edge},K} = \big[\mathbf{C}_h, \mathbf{C}_h\big]^{1/2}_{\mathrm{edge},K} \quad \forall \mathbf{C}_h \in \mathbf{V}_h^{\mathrm{edge}}(K). \tag{51}$$

Furthermore, the two following fundamental properties of $\mathbb{P}_0$-consistency and stability hold

- **Stability**: there exist two real constants β_* and $\beta^* > 0$ independent of h and K, such that

$$\beta_* \|\mathbf{C}_h\|_{0,K} \le |||\mathbf{C}_h|||_{\mathrm{edge},K} \le \beta^* \|\mathbf{C}_h\|_{0,K} \quad \forall \mathbf{C}_h \in \mathbf{V}_h^{\mathrm{edge}}(K). \tag{52}$$

- **Consistency**: for all $\mathbf{C}_h \in \mathbf{V}_h^{\mathrm{edge}}(K)$, it holds that

$$\big[\mathbf{C}_h, \mathbf{q}\big]_{\mathrm{edge},K} = \big(\mathbf{C}_h, \mathbf{q}\big)_K \quad \forall \mathbf{q} \in [\mathbb{P}_0(K)]^2 \tag{53}$$

We define the global virtual element space $\mathbf{V}_h^{\mathrm{edge}}$ by a conforming coupling if the elemental spaces $\mathbf{V}_h^{\mathrm{edge}}(K)$

$$\mathbf{V}_h^{\mathrm{edge}} = \Big\{ \mathbf{C}_h \in H(\mathrm{div}, \Omega) : \mathbf{C}_{h|K} \in \mathbf{V}_h^{\mathrm{edge}}(K)\ \forall K \in \Omega_h \Big\}.$$

We endow this space with the inner product

$$\big[\mathbf{B}_h, \mathbf{C}_h\big]_{\mathrm{edge}} = \sum_{K \in \Omega_h} \big[\mathbf{B}_h, \mathbf{C}_h\big]_{\mathrm{edge},K} \quad \forall \mathbf{B}_h, \mathbf{C}_h \in \mathbf{V}_h^{\mathrm{edge}}, \tag{54}$$

and the induced norm

$$|||\mathbf{C}_h|||^2_{\mathrm{edge}} = \big[\mathbf{C}_h, \mathbf{C}_h\big]_{\mathrm{edge}} \quad \forall \mathbf{C}_h \in \mathbf{V}_h^{\mathrm{edge}}. \tag{55}$$

The cell space. Finally, we introduce the local space of constant polynomials on each element K, i.e., $V_h^{\mathrm{cell}}(K) = \mathbb{P}_0(K)$, and the global space of piecewise constant polynomials on the mesh Ω_h

$$V_h^{\mathrm{cell}} = \Big\{ q_h \in L^2(\Omega) : q_{h|K} \in \mathbb{P}_0(K)\ \forall K \in \Omega_h \Big\}. \tag{56}$$

The degrees of freedom of a function $q_h \in V_h^{\text{cell}}$ are given by

(C) the elemental averages of q_h over every cell $K \in \Omega_h$

$$\frac{1}{|K|}\int_K q_h \, d\mathbf{x}.$$

These degrees of freedom are unisolvent in V_h^{cell}. We define the interpolation operator $\mathcal{I}_{\text{cell}} : L^2(\Omega) \to V_h^{\text{cell}}$ such that

$$\forall q \in L^2(\Omega): \quad \mathcal{I}_{\text{cell}}(q)_{|K} = \frac{1}{|K|}\int_K q \, d\mathbf{x}.$$

Fig. 1 (right panel) represents the degree of freedom associated with element K by an internal (red) disk.

We endow the cell space V_h^{cell} with the inner product

$$(p_h, q_h)_{\text{cell}} = \sum_K |K| \, p_K \, q_K \quad \forall p_h, q_h \in V_h^{\text{cell}},$$

which is the $L^2(\Omega)$ inner product of the two piecewise constant functions $p_h = (p_K)$ and $q_h = (q_K)$ defined on Ω_h, so that $p_K = p_{h|K}$, $q_K = q_{h|K}$. This inner product induces the norm

$$|\!|\!| q_h |\!|\!|_{\text{cell}} = (p_h, q_h)_{\text{cell}}^{\frac{1}{2}} \quad \forall q_h \in V_h^{\text{cell}},$$

which is the $L^2(\Omega)$-norm restricted to the functions of V_h^{cell}, so that

$$|\!|\!| q_h |\!|\!|_{\text{cell}} = \|q_h\|_{0,\Omega} \quad \forall q_h \in V_h^{\text{cell}}.$$

3.3. The de Rham complex

The spaces $H(\mathbf{rot}, \Omega)$, $H(\text{div}, \Omega)$ and $L^2(\Omega)$ form the well-known de Rham chain

$$H(\mathbf{rot}, \Omega) \xrightarrow{\mathbf{rot}} H(\text{div}, \Omega) \xrightarrow{\text{div}} L^2(\Omega). \tag{57}$$

If Ω is simply connected, the chain is exact, cf. [34]. Equivalently, we can say that

$$\mathbf{rot}\, H(\mathbf{rot}, \Omega) = \Big\{ \mathbf{C} \in H(\text{div}, \Omega) : \text{div}\, \mathbf{C} = 0 \Big\}.$$

The spaces V_h^{node}, $\mathbf{V}_h^{\text{edge}}$ and V_h^{cell} introduced in the previous section also form a similar exact de Rham chain

$$V_h^{\text{node}} \xrightarrow{\mathbf{rot}} \mathbf{V}_h^{\text{edge}} \xrightarrow{\text{div}} V_h^{\text{cell}}. \tag{58}$$

The chain (58), also shown in Fig. 1, was first introduced in [41], and explored in more detail and generality in [10]. Accordingly, the degrees of freedom of the virtual element spaces V_h^{node}, $\mathbf{V}_h^{\text{edge}}$ and V_h^{cell} transform as in the diagram depicted in Fig. 1. In fact, the two following main properties are satisfied

$$\mathbf{rot}\, V_h^{\text{node}} \subset \mathbf{V}_h^{\text{edge}} \tag{59}$$

$$\text{div}\, \mathbf{V}_h^{\text{edge}} \subset V_h^{\text{cell}} \tag{60}$$

Hence, if $D_h \in V_h^{\text{node}}$, then $\mathbf{rot}\, D_h \in \mathbf{V}_h^{\text{edge}}$, and we can compute the degrees of freedom of $\mathbf{rot}\, D_h$ in $\mathbf{V}_h^{\text{edge}}$ from the degrees of freedom of D_h in V_h^{node}. Consider an edge e in one of the cells in the mesh Ω_h. Then, the Theorem of Line Integrals implies that

$$\frac{1}{|e|}\int_e \mathbf{rot}\, D_h \cdot \mathbf{n} \, d\ell = \frac{1}{|e|}\int_e \nabla D_h \cdot \mathbf{t} \, d\ell = \frac{D_h(\mathbf{x}_2) - D_h(\mathbf{x}_1)}{|e|}, \tag{61}$$

where $\mathbf{x}_1$ and $\mathbf{x}_2$ are the coordinate vectors of the endpoint vertices of edge e. Thus, the degrees of freedom of V_h^{node} provide the necessary information to compute the image in $\mathbf{V}_h^{\text{edge}}$ of the rotational operator.

The same is true about the divergence of a vector-valued field in $\mathbf{V}_h^{\text{edge}}$. Let $K \in \Omega_h$ and consider $\mathbf{C}_h \in \mathbf{V}_h^{\text{edge}}$. Then, the Divergence Theorem implies that

$$\frac{1}{|K|}\int_K \text{div}\, \mathbf{C}_h \, d\mathbf{x} = \frac{1}{|K|}\int_{\partial K} \mathbf{C}_h \cdot \mathbf{n} d\ell = \frac{1}{|K|}\sum_{e \in \partial K}\int_e \mathbf{C}_h \cdot \mathbf{n}_e \, d\ell, \tag{62}$$

and we can compute the degrees of freedom of $\operatorname{div}\mathbf{C}_h$ in V_h^{cell} from the degrees of freedom of $\mathbf{C}_h$ in $\mathbf{V}_h^{\text{edge}}$. Thus, the degrees of freedom of $\mathbf{V}_h^{\text{edge}}$ provide the necessary information to compute the image in V_h^{cell} of the divergence operator.

These properties, summarized by Eqs. (61) and (62), are crucial to study the finite-dimensional spaces V_h^{node}, $\mathbf{V}_h^{\text{edge}}$ and V_h^{cell} and their relationship with the continuous larger spaces $H(\mathbf{rot}, \Omega)$, $H(\operatorname{div}, \Omega)$ and $L^2(\Omega)$. These spaces and the corresponding interpolation operators, i.e., $\mathcal{I}_{\text{node}}$, $\mathcal{I}_{\text{edge}}$, $\mathcal{I}_{\text{cell}}$, form the de Rham diagram

$$\begin{array}{ccccc} H(\mathbf{rot}, \Omega) & \xrightarrow{\mathbf{rot}} & H(\operatorname{div}, \Omega) & \xrightarrow{\operatorname{div}} & L^2(\Omega) \\ \downarrow{\scriptstyle \mathcal{I}_{\text{node}}} & & \downarrow{\scriptstyle \mathcal{I}_{\text{edge}}} & & \downarrow{\scriptstyle \mathcal{I}_{\text{cell}}} \\ V_h^{\text{node}} & \xrightarrow{\mathbf{rot}} & \mathbf{V}_h^{\text{edge}} & \xrightarrow{\operatorname{div}} & V_h^{\text{cell}}. \end{array} \tag{63}$$

This diagram is commutative, meaning that the following identities hold

$$\forall D \in H(\mathbf{rot}, \Omega): \quad \mathcal{I}_{\text{edge}} \circ \mathbf{rot}\,(D) = \mathbf{rot} \circ \mathcal{I}_{\text{node}}(D), \tag{64a}$$

$$\forall \mathbf{C} \in H(\operatorname{div}, \Omega): \quad \mathcal{I}_{\text{cell}} \circ \operatorname{div}(\mathbf{C}) = \operatorname{div} \circ \mathcal{I}_{\text{edge}}(\mathbf{C}). \tag{64b}$$

We summarize our findings in the following theorem.

Theorem 3.3. *The chain in (58) is well-defined and exact. Moreover, the diagram in (63) is commutative.*

4. Energy stability estimates

The conforming nature of VEM allows us to mimic many properties that are present in the continuous scenario. One of the more important is preserving certain types of estimates in the $L^2(\Omega)-$norm. These usually come about after testing the variational formulation against the exact solution and applying the Gronwall's Lemma, see [23]. In this section, we present an estimate of this type, true for the solutions to the continuous variational formulation (11), and its discrete virtual element counterpart! (19).

Let $\mathbf{u}_b$ and E_b denote the liftings of the boundary functions $\mathbf{u}_b^\partial$ and E_b^∂ that we introduced in (9) in $\left[H^1(\Omega)\right]^2$ and $H(\mathbf{rot}, \Omega)$, respectively, with the assumption that $\operatorname{div}\mathbf{u}_b = 0$. In order to reveal the boundary information, we consider the decompositions

$$\mathbf{u} = \hat{\mathbf{u}} + \mathbf{u}_b \quad \text{and} \quad E = \hat{E} + E_b, \tag{65}$$

where $\hat{\mathbf{u}} \in \left[H_0^1(\Omega)\right]^2$ and $\widehat{E} \in H_0(\mathbf{rot}, \Omega)$. Since $\operatorname{div}\mathbf{u}_b = 0$, Eq. (65) and the divergence-free nature of $\mathbf{u}$ imply that $\operatorname{div}\hat{\mathbf{u}} = 0$. Next, using (65) we write $j = \hat{j} + j_b$ where

$$\hat{j} = \widehat{E} + \hat{\mathbf{u}} \times \mathbf{B} \quad \text{and} \quad j_b = E_b + \mathbf{u}_b \times \mathbf{B}. \tag{66}$$

We state the continuous energy estimate in the following theorem, whose proof is reported for completeness. Similar estimates can be found in [26,28,29].

Lemma 4.1. *Let $(\mathbf{u}, \mathbf{B}, E, p)$ solve the variational formulation (11) in the time interval $[0, T]$. Then, we have the equality*

$$\begin{aligned} &\frac{1}{2}\frac{d}{dt}\|\hat{\mathbf{u}}\|_{0,\Omega}^2 + \frac{s}{2}R_m^{-1}\frac{d}{dt}\|\mathbf{B}\|_{0,\Omega}^2 + R_e^{-1}\|\nabla\hat{\mathbf{u}}\|_{0,\Omega}^2 + s\|\hat{j}\|_{0,\Omega}^2 \\ &\quad = (\mathbf{f}, \hat{\mathbf{u}}) - \left(\mathbf{u}_{b,t}, \hat{\mathbf{u}}\right) - R_e^{-1}(\nabla\mathbf{u}_b, \nabla\hat{\mathbf{u}}) - sR_m^{-1}(\mathbf{rot}\,E_b, \mathbf{B}) - s(j_b, \hat{j}), \end{aligned} \tag{67}$$

with the notation $\mathbf{u}_{b,t} = \partial\mathbf{u}_b/\partial t$.

Proof. We set $(\mathbf{v}, \mathbf{C}, F, q) = (\hat{\mathbf{u}}, \mathbf{B}, \widehat{E}, p)$ in (11a)–(11d). Since $\operatorname{div}\hat{\mathbf{u}} = 0$, $(j_h \times \mathbf{B}, \hat{\mathbf{u}}) = -(j_h, \hat{\mathbf{u}} \times \mathbf{B})$, $j_h = \hat{j} + j_b$, cf. (66), and using the notation $\mathbf{u}_{b,t} = \partial\mathbf{u}_b/\partial t$, we find that

$$\begin{aligned} \frac{1}{2}\frac{d}{dt}\|\hat{\mathbf{u}}\|_{0,\Omega}^2 + R_e^{-1}\|\nabla\hat{\mathbf{u}}\|_{0,\Omega}^2 + s(\hat{j}, \hat{\mathbf{u}} \times \mathbf{B}) &= (\mathbf{f}, \hat{\mathbf{u}}) - (\mathbf{u}_{b,t}, \hat{\mathbf{u}}) - R_e^{-1}(\nabla\mathbf{u}_b, \nabla\hat{\mathbf{u}}) \\ &\quad - s(j_b, \hat{\mathbf{u}} \times \mathbf{B}), \end{aligned} \tag{68a}$$

$$\frac{s}{2}R_m^{-1}\frac{d}{dt}\|\mathbf{B}\|_{0,\Omega}^2 + sR_m^{-1}(\mathbf{rot}\,\hat{E},\mathbf{B}) = -sR_m^{-1}(\mathbf{rot}\,E_b,\mathbf{B}), \tag{68b}$$

$$s(\hat{j},\hat{E}) - sR_m^{-1}(\mathbf{B},\mathbf{rot}\,\hat{E}) = -s(j_b,\widehat{E}). \tag{68c}$$

Adding Eqs. (68a), (68b), and (68c) yields the equality (67). □

Theorem 4.2. *Under the assumptions of Lemma 4.1, as a consequence of equality (67), we have the following estimate*

$$\begin{aligned}\|\hat{\mathbf{u}}(T)\|_{0,\Omega}^2 + sR_m^{-1}\|\mathbf{B}(T)\|_{0,\Omega}^2 + \int_0^T e^{(T-t)}\left(R_e^{-1}\|\nabla\hat{\mathbf{u}}\|_{0,\Omega}^2 + s\|\hat{j}\|_{0,\Omega}^2\right)dt \\ \le \|\hat{\mathbf{u}}(0)\|_{0,\Omega}^2 + R_m^{-1}\|\mathbf{B}(0)\|_{0,\Omega}^2 + \int_0^T e^{(T-t)}\Big(\,2R_e\|\mathbf{f}\|_{-1,\Omega}^2 + \|\mathbf{u}_{b,t}\|_{0,\Omega}^2 \\ + 2R_e^{-1}\|\nabla\mathbf{u}_b\|_{0,\Omega}^2 + sR_m^{-1}\|\mathbf{rot}\,E_b\|_{0,\Omega}^2 + s\|j_b\|_{0,\Omega}^2\Big)\,dt.\end{aligned} \tag{69}$$

Proof. To obtain inequality (69) from equality (67) we first take the absolute value on the right-hand side of (67) and use the triangle inequality to obtain

$$\begin{aligned}&\frac{1}{2}\frac{d}{dt}\|\hat{\mathbf{u}}\|_{0,\Omega}^2 + \frac{s}{2}R_m^{-1}\frac{d}{dt}\|\mathbf{B}\|_{0,\Omega}^2 + R_e^{-1}\|\nabla\hat{\mathbf{u}}\|_{0,\Omega}^2 + s\|\hat{j}\|_{0,\Omega}^2 \\ &\quad\le |(\mathbf{f},\hat{\mathbf{u}})| + |(\mathbf{u}_{b,t},\hat{\mathbf{u}})| + R_e^{-1}|(\nabla\mathbf{u}_b,\nabla\hat{\mathbf{u}})| + sR_m^{-1}|(\mathbf{rot}\,E_b,\mathbf{B}) + s|(j_b,\hat{j})||.\end{aligned} \tag{70}$$

We bound the right-hand side of (70) using the following Young's inequalities:

$$\left|(\mathbf{f},\hat{\mathbf{u}})\right| \le \|\mathbf{f}\|_{-1,\Omega}\|\nabla\hat{\mathbf{u}}\|_{0,\Omega} \le R_e\|\mathbf{f}\|_{-1,\Omega}^2 + \frac{1}{4}R_e^{-1}\|\nabla\hat{\mathbf{u}}\|_{0,\Omega}^2, \tag{71a}$$

$$\left|(\mathbf{u}_{b,t},\hat{\mathbf{u}})\right| \le \frac{1}{2}\|\mathbf{u}_{b,t}\|_{0,\Omega}^2 + \frac{1}{2}\|\hat{\mathbf{u}}\|_{0,\Omega}^2, \tag{71b}$$

$$R_e^{-1}\left|(\nabla\mathbf{u}_b,\nabla\hat{\mathbf{u}})\right| \le R_e^{-1}\frac{1}{2}\|\nabla\mathbf{u}_b\|_{0,\Omega}^2 + R_e^{-1}\frac{1}{2}\|\nabla\hat{\mathbf{u}}\|_{0,\Omega}^2, \tag{71c}$$

$$sR_m^{-1}\left|(\mathbf{rot}\,E_b,\mathbf{B})\right| \le R_m^{-1}\frac{s}{2}\|\mathbf{rot}\,E_b\|_{0,\Omega}^2 + R_m^{-1}\frac{s}{2}\|\mathbf{B}\|_{0,\Omega}^2, \tag{71d}$$

$$s\left|(j_b,\hat{j})\right| \le \frac{s}{2}\|j_b\|_{0,\Omega}^2 + \frac{s}{2}\|\hat{j}\|_{0,\Omega}^2. \tag{71e}$$

Substituting (71) into the RHS of (70) and rearranging the terms, yields,

$$\begin{aligned}&\frac{d}{dt}\left(\frac{1}{2}\|\hat{\mathbf{u}}\|_{0,\Omega}^2 + \frac{s}{2}R_m^{-1}\|\mathbf{B}\|_{0,\Omega}^2\right) - \left(\frac{1}{2}\|\hat{\mathbf{u}}\|_{0,\Omega}^2 + \frac{s}{2}R_m^{-1}\|\mathbf{B}\|_{0,\Omega}^2\right) + \frac{1}{2}R_e^{-1}\|\nabla\hat{\mathbf{u}}\|_{0,\Omega}^2 + \frac{s}{2}\|\hat{j}\|_{0,\Omega}^2 \\ &\qquad\le R_e\|\mathbf{f}\|_{-1,\Omega}^2 + \frac{1}{2}\|\mathbf{u}_{b,t}\|_{0,\Omega}^2 + R_e^{-1}\|\nabla\mathbf{u}_b\|_{0,\Omega}^2 + \frac{s}{2}R_m^{-1}\|\mathbf{rot}\,E_b\|_{0,\Omega}^2 + \frac{s}{2}\|j_b\|_{0,\Omega}^2.\end{aligned} \tag{72}$$

Note that

$$\begin{aligned}&\frac{d}{dt}e^{-t}\left(\|\hat{\mathbf{u}}\|_{0,\Omega}^2 + sR_m^{-1}\|\mathbf{B}\|_{0,\Omega}^2\right) \\ &\qquad= e^{-t}\frac{d}{dt}\left(\|\hat{\mathbf{u}}\|_{0,\Omega}^2 + sR_m^{-1}\|\mathbf{B}\|_{0,\Omega}^2\right) - e^{-t}\left(\|\hat{\mathbf{u}}\|_{0,\Omega}^2 + sR_m^{-1}\|\mathbf{B}\|_{0,\Omega}^2\right).\end{aligned} \tag{73}$$

Multiplying (72) by $2e^{-t}$ and using (73) we get

$$\begin{aligned}&\frac{d}{dt}e^{-t}\left(\|\hat{\mathbf{u}}\|_{0,\Omega}^2 + sR_m^{-1}\|\mathbf{B}\|_{0,\Omega}^2\right) + e^{-t}\left(R_e^{-1}\|\nabla\hat{\mathbf{u}}\|_{0,\Omega}^2 + s\|\hat{j}\|_{0,\Omega}^2\right) \le 2e^{-t}R_e\|\mathbf{f}\|_{-1,\Omega}^2 \\ &\quad + e^{-t}\|\mathbf{u}_{b,t}\|_{0,\Omega}^2 + 2e^{-t}R_e^{-1}\|\nabla\mathbf{u}_b\|_{0,\Omega}^2 + se^{-t}R_m^{-1}\|\mathbf{rot}\,E_b\|_{0,\Omega}^2 + se^{-t}\|j_b\|_{0,\Omega}^2,\end{aligned} \tag{74}$$

Finally, we integrate (74) in time over $[0,T]$ and multiply by e^T to obtain estimate (69). □

To obtain a discrete version of the estimate of Theorem 4.2, we consider the decomposition of the electric and the velocity fields E_h^{n+1} and $\mathbf{u}_h^{n+1}$ into the deterministic boundary components $\mathcal{I}_{\text{node}}(E_b)$ and $\mathfrak{I}(\mathbf{u}_b)$ and the internal

components $\hat{E}_h^{n+1}$ and $\hat{\mathbf{u}}_h^{n+1}$:

$$E_h^{n+1} = \hat{E}_h^{n+1} + \mathcal{I}_{\text{node}}(E_b) \quad \text{and} \quad \mathbf{u}_h^{n+1} = \hat{\mathbf{u}}_h^{n+1} + \mathfrak{I}(\mathbf{u}_b), \tag{75}$$

where the integer n for $1 \le n \le N$ is the time step index, and $\mathfrak{I}$ is the interpolation operator of Definition 3.1.

In (75), we have that $\hat{E}^{n+1} \in V_{0,h}^{\text{node}}$. Next, for all integers $1 \le n \le N$, we introduce the discrete current densities

$$\hat{j}_h^n := \widetilde{\Pi}\hat{E}^n + \Pi^0\hat{\mathbf{u}}_h^n \times \Pi^0\mathbf{B}_h^n \qquad \text{and} \qquad j_{h,b}^n := \widetilde{\Pi}\mathcal{I}_{\text{node}}E_b + \Pi^0\mathfrak{I}\mathbf{u}_b \times \Pi^0\mathbf{B}_h^n, \tag{76}$$

so that

$$j_h^n = \hat{j}_h^n + j_{h,b}^n = \widetilde{\Pi}E_h^n + \Pi^0\mathbf{u}_h^n \times \Pi^0\mathbf{B}_h^n,$$

as defined in (18), which by definition is a piecewise constant field on the elements of Ω_h. Lemma 4.3 and Theorem 4.3 are the discrete analogs of Lemma 4.1 and Theorem 4.2.

Lemma 4.3. *Let* $\{(\mathbf{u}_h^n, \mathbf{B}_h^n, E_h^n, p_h^n)\}_{n=1}^N \in \mathbf{W}_h \times \mathbf{V}_h^{\text{edge}} \times V_h^{\text{node}} \times Q_h$ *solve the discrete formulation (19) with* $\mathbf{u}_{h,0} = \mathfrak{I}(\mathbf{u}_0)$ *and* $\mathbf{B}_{h,0} = \mathcal{I}_{\text{edge}}(\mathbf{B}_0)$. *Then, we have the following equality*

$$\mathcal{L}_0 + \mathcal{L}_1 + \mathcal{L}_2 = \mathcal{R}, \tag{77}$$

where

$$\mathcal{L}_0 := \left(\frac{\|\hat{\mathbf{u}}_h^{n+1} - \hat{\mathbf{u}}_h^n\|_{\mathbf{W}_h}^2}{2\Delta t} + R_m^{-1}\frac{\|\mathbf{B}_h^{n+1} - \mathbf{B}_h^n\|_{\text{edge}}^2}{2\Delta t} \right),$$

$$\mathcal{L}_1 := \left(\frac{\|\hat{\mathbf{u}}_h^{n+1}\|_{\mathbf{W}_h}^2 - \|\hat{\mathbf{u}}_h^n\|_{\mathbf{W}_h}^2}{2\Delta t} + R_m^{-1}\frac{\|\mathbf{B}_h^{n+1}\|_{\text{edge}}^2 - \|\mathbf{B}_h^n\|_{\text{edge}}^2}{2\Delta t} \right), \tag{78a}$$

$$\mathcal{L}_2 := R_e^{-1}a_h\big(\hat{\mathbf{u}}_h^{n+1}, \hat{\mathbf{u}}_h^{n+1}\big) + \|\hat{j}_h^{n+1}\|_{0,\Omega}^2 + \mathcal{S}^V\ \big(\ (\mathcal{I} - \tag{78b}$$

$$Pi\,Obl)\hat{E}_h^{n+1}, (\mathcal{I} - \widetilde{\Pi})\hat{E}_h^{n+1}\ \big), \tag{78c}$$

$$\mathcal{R} := m_h\big(\mathbf{f}_h^{n+1}, \hat{\mathbf{u}}_h^{n+1}\big) - R_e^{-1}a_h\big(\mathfrak{I}\mathbf{u}_b, \hat{\mathbf{u}}_h^{n+1}\big) - R_m^{-1}\big[\mathbf{rot}\,\mathcal{I}_{\text{node}}E_b, \mathbf{B}_h^{n+1}\big]_{\text{edge}}$$
$$- \big(j_{h,b}^{n+1}, \hat{j}_h^{n+1}\big) - \mathcal{S}^V\big((\mathcal{I} - \widetilde{\Pi})\mathcal{I}_{\text{node}}(E_b), (\mathcal{I} - \widetilde{\Pi})\hat{E}_h^{n+1}\big). \tag{78d}$$

Proof. We set $(\mathbf{v}_h, \mathbf{C}_h, F_h, q_h) = (\hat{\mathbf{u}}_h^{n+1}, \mathbf{B}_h^{n+1}, \hat{E}_h^{n+1}, p_h^{n+1})$ in (19a)–(19d) at the discrete time t^{n+1}. Using decompositions (75) we obtain

$$m_h\left(\frac{\hat{\mathbf{u}}_h^{n+1} - \hat{\mathbf{u}}_h^n}{\Delta t}, \hat{\mathbf{u}}_h^{n+1}\right) + R_e^{-1}a_h\big(\hat{\mathbf{u}}_h^{n+1}, \hat{\mathbf{u}}_h^{n+1}\big) - b\big(\hat{\mathbf{u}}_h^{n+1}, p_h^{n+1}\big)$$
$$+ \big(\hat{j}_h^{n+1}, \Pi^0\hat{\mathbf{u}}_h^{n+1} \times \Pi^0\mathbf{B}_h^{n+1}\big) = m_h\big(\mathbf{f}_h^{n+1}, \hat{\mathbf{u}}_h^{n+1}\big) - R_e^{-1}a_h\big(\mathfrak{I}\mathbf{u}_b, \hat{\mathbf{u}}_h^{n+1}\big) \tag{79a}$$
$$- \big(j_{h,b}^{n+1}, \Pi^0\hat{\mathbf{u}}_h^{n+1} \times \Pi^0\mathbf{B}_h^{n+1}\big),$$

$$\big[E_h^{n+1}, \hat{E}_h^{n+1}\big]_{\text{node}} + (\Pi^0\mathbf{u}_h^{n+1} \times \Pi^0\mathbf{B}_h^{n+1}, \widetilde{\Pi}\hat{E}_h^{n+1})R_m^{-1}\big[\mathbf{B}_h^{n+1}, \mathbf{rot}\,\hat{E}_h^{n+1}\big]_{\text{edge}} = 0, \tag{79b}$$

$$R_m^{-1}\left[\frac{\mathbf{B}_h^{n+1} - \mathbf{B}_h^n}{\Delta t}, \mathbf{B}_h^{n+1}\right]_{\text{edge}} + R_m^{-1}\big[\mathbf{rot}\,\hat{E}_h^{n+1}, \mathbf{B}_h^{n+1}\big]_{\text{edge}}$$
$$= -R_m^{-1}\big[\mathbf{rot}\,\mathcal{I}_{\text{node}}E_b^{n+1}, \mathbf{B}_h^{n+1}\big]_{\text{edge}}, \tag{79c}$$

$$b\big(\mathbf{u}_h^{n+1}, p_h^{n+1}\big) = 0. \tag{79d}$$

We will now focus on Eq. (79b). The first term in Eq. (79b), based on (42), admits the decomposition

$$\big[E_h^{n+1}, \hat{E}_h^{n+1}\big]_{\text{node}} = \big(\ \Pi E_h^{n+1}, \widetilde{\Pi}\hat{E}_h^{n+1}\big) + \mathcal{S}^V\big((\mathcal{I} - \widetilde{\Pi})E_h^{n+1}, (\mathcal{I} - \widetilde{\Pi})\hat{E}_h^{n+1}\big). \tag{80}$$

Grouping the first term in (80) with the second term in (79b) we get

$$\begin{aligned}\big(\widetilde{\Pi}E_h^{n+1}, \widetilde{\Pi}\hat{E}_h^{n+1}\big) + \big(\Pi^0\mathbf{u}_h^{n+1} \times \Pi^0\mathbf{B}_h^{n+1}, \widetilde{\Pi}\hat{E}_h^{n+1}\big) \\ = \big(\widetilde{\Pi}E_h^{n+1} + \Pi^0\mathbf{u}_h^{n} \times \Pi^0\mathbf{B}_h^{n}, \widetilde{\Pi}\hat{E}_h^{n+1}\big) \\ = \big(j_h^{n+1}, \widetilde{\Pi}\hat{E}_h^{n+1}\big) = \big(\hat{j}_h^{n+1} + j_{h,b}^{n+1}, \widetilde{\Pi}\hat{E}_h^{n+1}\big).\end{aligned} \tag{81}$$

Thus, Eq. (79b) takes form

$$\begin{aligned}\mathcal{S}^V\big((\mathcal{I} - \widetilde{\Pi})E_h^{n+1}, (\mathcal{I} - \widetilde{\Pi})\hat{E}_h^{n+1}\big) + \big(\hat{j}_h^{n+1} + j_{h,b}^{n+1}, \widetilde{\Pi}\hat{E}_h^{n+1}\big) \\ - R_m^{-1}\big[\mathbf{B}_h^{n+1}, \mathbf{rot}\,\hat{E}_h^{n+1}\big]_{\text{edge}} = 0.\end{aligned} \tag{82}$$

Using property of the interpolation operator $\mathfrak{I}$ of preserving the value of the bilinear form $b(\mathbf{u}, p_h)$ and the weak divergence free property of the boundary lifting term $\mathbf{u}_b$ we have

$$b\big(\mathfrak{I}\mathbf{u}_b, p_h^{n+1}\big) = b\big(\mathbf{u}_b, p_h^{n+1}\big) = 0. \tag{83}$$

Moreover, a straightforward calculation using the identity $2(a-b)a = (a-b)^2 + a^2 - b^2$ shows that

$$m_h\left(\frac{\hat{\mathbf{u}}_h^{n+1} - \hat{\mathbf{u}}_h^{n}}{\Delta t}, \hat{\mathbf{u}}_h^{n+1}\right) = \frac{|||\hat{\mathbf{u}}_h^{n+1} - \hat{\mathbf{u}}_h^{n}|||_{\mathbf{W}_h}^2}{2\Delta t} + \frac{|||\hat{\mathbf{u}}^{n+1}|||_{\mathbf{W}_h}^2 - |||\hat{\mathbf{u}}^{n}|||_{\mathbf{W}_h}^2}{2\Delta t}, \tag{84a}$$

$$\left[\frac{\mathbf{B}_h^{n+1} - \mathbf{B}_h^{n}}{\Delta t}, \mathbf{B}_h^{n+1}\right]_{\text{edge}} = \frac{|||\mathbf{B}_h^{n+1} - \mathbf{B}_h^{n}|||_{\text{edge}}^2}{2\Delta t} + \frac{|||\mathbf{B}_h^{n+1}|||_{\text{edge}}^2 - \|\mathbf{B}_h^{n}\|_{\text{edge}}^2}{2\Delta t}. \tag{84b}$$

Adding Eqs. (79a), (82), (79c)–(79d), using (83) and (84a)–(84b) yield (78). □

Theorem 4.4. *Under the assumptions of Lemma 4.3, as a consequence of equality (78), we have the following energy stability estimate*

$$\begin{aligned}|||\hat{\mathbf{u}}_h^N|||_{\mathbf{W}_h}^2 + R_m^{-1}|||\mathbf{B}_h^N|||_{\text{edge}}^2 \le (1+\Delta t)^N\Big[|||\hat{\mathbf{u}}_h^0|||_{\mathbf{W}_h}^2 + R_m^{-1}|||\mathbf{B}_h^0|||_{\text{edge}}^2\Big] \\ + 2\Delta t\sum_{n=0}^{N-1}(1+\Delta t)^{N-(n+1)}\mathcal{F}^{n+1}(\mathbf{f}_h^{n+1}, \mathbf{u}_b, E_b),\end{aligned} \tag{85}$$

where

$$\begin{aligned}\mathcal{F}^{n+1}(\mathbf{f}_h^{n+1}, \mathbf{u}_b, E_b) \coloneqq \frac{1}{2}R_e|||\mathbf{f}_h^{n+1}|||_{-1,\Omega}^2 + \frac{1}{2}R_e^{-1}a_h(\mathfrak{I}\mathbf{u}_b, \mathfrak{I}\mathbf{u}_b) \\ + \frac{1}{2}R_m^{-1}|||\mathbf{rot}\,\mathcal{I}_{\text{node}}E_b|||_{\text{edge}}^2 + \frac{1}{2}\|j_{h,b}^{n+1}\|_{0,\Omega}^2 \\ + \frac{1}{4}\mathcal{S}^V\big((\mathcal{I} - \widetilde{\Pi})\mathcal{I}_{\text{node}}(E_b), (\mathcal{I} - \widetilde{\Pi})\mathcal{I}_{\text{node}}(E_b)\big).\end{aligned} \tag{86}$$

Proof. We first note that

$$\mathcal{L}_0 = \frac{1}{2\Delta t}\left(|||\hat{\mathbf{u}}_h^{n+1} - \hat{\mathbf{u}}_h^{n}|||_{\mathbf{W}_h}^2 + |||\mathbf{B}_h^{n+1} - \mathbf{B}_h^{n}|||_{\text{edge}}^2\right) \ge 0.$$

Thus, the demonstrated equality (78) implies that

$$\mathcal{L}_1 = \mathcal{L}_1^{\hat{\mathbf{u}}_h} + \mathcal{L}_1^{\mathbf{B}_h} \le |\mathcal{R}| - \mathcal{L}_2, \tag{87}$$

where

$$\mathcal{L}_1^{\hat{\mathbf{u}}_h} = \frac{1}{2}\frac{|||\hat{\mathbf{u}}_h^{n+1}|||_{\mathbf{W}_h}^2 - |||\hat{\mathbf{u}}_h^{n}|||_{\mathbf{W}_h}^2}{\Delta t}, \qquad \mathcal{L}_1^{\mathbf{B}_h} = \frac{1}{2}R_m^{-1}\frac{|||\mathbf{B}_h^{n+1}|||_{\text{edge}}^2 - \|\mathbf{B}_h^{n}\|_{\text{edge}}^2}{\Delta t},$$

and

$$\begin{aligned}|\mathcal{R}| \le \big|m_h\big(\mathbf{f}_h^{n+1}, \hat{\mathbf{u}}_h^{n+1}\big)\big| + R_e^{-1}\big|a_h\big(\mathfrak{I}\mathbf{u}_b, \hat{\mathbf{u}}_h^{n+1}\big)\big| + R_m^{-1}\Big|\big[\mathbf{rot}\,\mathcal{I}_{\text{node}}E_b, \mathbf{B}_h^{n+1}\big]_{\text{edge}}\Big| \\ + \Big|\big(j_{h,b}^{n+1}, \hat{j}_h^{n+1}\big)\Big| + \Big|\mathcal{S}^V\big((\mathcal{I} - \widetilde{\Pi})\mathcal{I}_{\text{node}}(E_b), (\mathcal{I} - \widetilde{\Pi})\hat{E}_h^{n+1}\big)\Big|.\end{aligned} \tag{88}$$

The term $|\mathcal{R}|$ contains mixed terms, while $\mathcal{L}_2$ contains quadratic terms only. Our strategy will be to estimate each of the terms in the RHS of (88) using Young's inequalities so that the quadratic terms for the solution functions $\hat{\mathbf{u}}_h^{n+1}$, $\mathbf{B}_h^{n+1}$ and $\hat{E}_h^{n+1}$ that come out cancel with the corresponding quadratic terms in $\mathcal{L}_2$, see (78b):

$$\left|m_h(\mathbf{f}_h^{n+1}, \hat{\mathbf{u}}_h^{n+1})\right| \leq \frac{1}{2} R_e \|\mathbf{u}_h^{n+1}\|_{-1,\Omega}^2 + \frac{1}{2} R_e^{-1} a_h(\hat{\mathbf{u}}_h^{n+1}, \hat{\mathbf{u}}_h^{n+1}), \tag{89a}$$

$$\left|R_e^{-1} a_h(\mathfrak{I}\mathbf{u}_b, \hat{\mathbf{u}}_h^{n+1})\right| \leq \frac{1}{2} R_e^{-1} a_h(\mathfrak{I}\mathbf{u}_b, \mathfrak{I}\mathbf{u}_b) + \frac{1}{2} R_e^{-1} a_h(\hat{\mathbf{u}}_h^{n+1}, \hat{\mathbf{u}}_h^{n+1}), \tag{89b}$$

$$R_m^{-1} \left|\left[\mathbf{rot}\, \mathcal{I}_{\text{node}} E_b, \mathbf{B}_h^{n+1}\right]_{\text{edge}}\right| \leq \frac{1}{2} R_m^{-1} \|\mathbf{rot}\, \mathcal{I}_{\text{node}} E_b\|_{\text{edge}}^2 + \frac{1}{2} R_m^{-1} \|\mathbf{B}_h^{n+1}\|_{\text{edge}}^2, \tag{89c}$$

$$\left|(j_{h,b}^{n+1}, \hat{j}_h^{n+1})\right| \leq \frac{1}{2} \|j_{h,b}^{n+1}\|_{0,\Omega}^2 + \frac{1}{2} \|\hat{j}_h^{n+1}\|_{0,\Omega}^2, \tag{89d}$$

$$\begin{aligned}\left|\mathcal{S}^V\left((\mathcal{I} - \widetilde{\Pi})\mathcal{I}_{\text{node}}(E_b), (\mathcal{I} - \widetilde{\Pi})\hat{E}_h^{n+1}\right)\right| \\ \leq \frac{1}{4} \mathcal{S}^V\left((\mathcal{I} - \widetilde{\Pi})\mathcal{I}_{\text{node}}(E_b), (\mathcal{I} - \widetilde{\Pi})\mathcal{I}_{\text{node}}(E_b)\right) \\ + \mathcal{S}^V\left((\mathcal{I} - \widetilde{\Pi})\hat{E}_h^{n+1}, (\mathcal{I} - \widetilde{\Pi})\hat{E}_h^{n+1}\right).\end{aligned} \tag{89e}$$

For the first term on the RHS of (89e) we use the upper bound property (50) of the stabilization term and the property of the projection operator

$$\mathcal{S}^V\left((\mathcal{I} - \widetilde{\Pi})\mathcal{I}_{\text{node}}(E_b), (\mathcal{I} - \widetilde{\Pi})\mathcal{I}_{\text{node}}(E_b)\right) \leq s^* \|(\mathcal{I} - \widetilde{\Pi})E_b\|^2 \leq s^* \|E_b\|^2. \tag{90}$$

We note that when substituting inequalities (89) into (87) all terms in $\mathcal{L}_2$ cancel exactly. The only term on the RHS of (89) that does not cancel and depends on the solution function is $\frac{1}{2} R_m^{-1} \|\mathbf{B}_h^{n+1}\|_{\text{edge}}^2$ in inequality (89c). To control this term we will move it to the LHS of (87) and combine it with $\mathcal{L}_1^{\mathbf{B}_h}$ to get a modified version of $\mathcal{L}_1^{\mathbf{B}_h}$:

$$\widetilde{\mathcal{L}_1^{\mathbf{B}_h}} := \frac{1}{2} R_m^{-1} \frac{\|\mathbf{B}_h^{n+1}\|_{\text{edge}}^2 - (1 + \Delta t)\|\mathbf{B}_h^n\|_{\text{edge}}^2}{\Delta t}. \tag{91}$$

For convenience purpose we will now consider a modified version of $\mathcal{L}_1^{\hat{\mathbf{u}}_h}$ analogous to (91):

$$\widetilde{\mathcal{L}_1^{\hat{\mathbf{u}}_h}} := \frac{1}{2} \frac{\|\hat{\mathbf{u}}_h^{n+1}\|_{\mathbf{W}_h}^2 - (1 + \Delta t)\|\hat{\mathbf{u}}_h^n\|_{\mathbf{W}_h}^2}{\Delta t} \tag{92}$$

and note that

$$\widetilde{\mathcal{L}_1^{\hat{\mathbf{u}}_h}} \leq \mathcal{L}_1^{\hat{\mathbf{u}}_h}. \tag{93}$$

Substituting the modified $\widetilde{\mathcal{L}_1^{\hat{\mathbf{u}}_h}}$ and $\widetilde{\mathcal{L}_1^{\mathbf{B}_h}}$ into (87) we get the following estimate

$$\widetilde{\mathcal{L}_1^{\hat{\mathbf{u}}_h}} + \widetilde{\mathcal{L}_1^{\mathbf{B}_h}} \leq \mathcal{F}^{n+1}(\mathbf{f}_h^{n+1}, \mathbf{u}_b, E_b), \tag{94}$$

where

$$\begin{aligned}\mathcal{F}^{n+1}(\mathbf{f}_h^{n+1}, \mathbf{u}_b, E_b) :=& \frac{1}{2} R_e \|\mathbf{f}_h^{n+1}\|_{-1,\Omega}^2 + \frac{1}{2} R_e^{-1} a_h(\mathfrak{I}\mathbf{u}_b, \mathfrak{I}\mathbf{u}_b) \\ &+ \frac{1}{2} R_m^{-1} \|\mathbf{rot}\, \mathcal{I}_{\text{node}} E_b\|_{\text{edge}}^2 + \frac{1}{2} \|j_{h,b}^{n+1}\|_{0,\Omega}^2 \\ &+ \frac{1}{4} \mathcal{S}^V\left((\mathcal{I} - \widetilde{\Pi})\mathcal{I}_{\text{node}}(E_b), (\mathcal{I} - \widetilde{\Pi})\mathcal{I}_{\text{node}}(E_b)\right).\end{aligned} \tag{95}$$

To obtain an estimate on $\|\mathbf{B}_h^N\|_{\text{edge}}^2$ and $\|\hat{\mathbf{u}}_h^N\|_{\mathbf{W}_h}^2$ after N integration time steps, multiply inequality (94) by $(1+\Delta t)^{N-n-1}$ and sum over all $n = 0, 1, \dots N-1$ to form a telescopic series on the LHS. Indeed,

$$\begin{aligned}
&\sum_{n=0}^{N-1}(1+\Delta t)^{N-n-1}\frac{\|\mathbf{B}_h^{n+1}\|_{\text{edge}}^2-(1+\Delta t)\|\mathbf{B}_h^n\|_{\text{edge}}^2}{\Delta t}\\
&\quad=\frac{1}{\Delta t}\sum_{n=0}^{N-1}(1+\Delta t)^{N-n-1}\|\mathbf{B}_h^{n+1}\|_{\text{edge}}^2-\frac{1}{\Delta t}\sum_{n=0}^{N-1}(1+\Delta t)^{N-n}\|\mathbf{B}_h^n\|_{\text{edge}}^2\\
&\quad=\frac{1}{\Delta t}\|\mathbf{B}_h^N\|_{\text{edge}}^2-\frac{1}{\Delta t}(1+\Delta t)^N\|\mathbf{B}_h^0\|_{\text{edge}}^2. \qquad (96)
\end{aligned}$$

Similarly,

$$\begin{aligned}
&\sum_{n=0}^{N-1}(1+\Delta t)^{N-n-1}\frac{\|\hat{\mathbf{u}}_h^{n+1}\|_{\mathbf{W}_h}^2-(1+\Delta t)\|\hat{\mathbf{u}}_h^n\|_{\mathbf{W}_h}^2}{\Delta t}\\
&\quad=\frac{1}{\Delta t}\|\hat{\mathbf{u}}_h^N\|_{\mathbf{W}_h}^2-\frac{1}{\Delta t}(1+\Delta t)^N\|\hat{\mathbf{u}}_h^0\|_{\mathbf{W}_h}^2. \qquad (97)
\end{aligned}$$

Using the results of the telescoping series (96) and (97), remembering the coefficients $\frac{1}{2}R_m^{-1}$ and $\frac{1}{2}$ in (91) and (92), respectively, and summing up $(1+\Delta t)^{N-n-1}\mathcal{F}^{n+1}(\mathbf{f}_h^{n+1}, \mathbf{u}_b, E_b)$ we get the desired estimate (85). □

Remark 4.1. The factor $(1+\Delta t)^N$ on the RHS of (85) approaches e^T for a fixed time integration window T and the number N of time integration steps going to infinity:

$$(1+\Delta t)^N=\left(1+\frac{T}{N}\right)^N=\left(1+\frac{T}{N}\right)^{\frac{N}{T}T}\to e^T \quad \text{as } N\to\infty.$$

5. Linearization

The semi-discrete form in (19) requires further treatment in order to provide computable approximations to the flow of the magnetized fluid. Precisely, we need a linearization strategy to handle the non-linear terms that appear in the time discretization. The approach we follow in this section is similar to the linearizations proposed, e.g., in [6,25,45]. The central idea is to make an "educated guess" $\mathbf{B}_{h,*}^n$ for the value of $\mathbf{B}_h^n$, so that we can approximate the three non-linear terms in (19) as follows:

$$\begin{aligned}
\left(\widetilde{\Pi}E_h^n, \Pi^0\mathbf{v}_h\times\Pi^0\mathbf{B}_h^n\right)&\approx\left(\widetilde{\Pi}E_h^n, \Pi^0\mathbf{v}_h\times\Pi^0\mathbf{B}_{h,*}^n\right) &(98)\\
\left(\Pi^0\mathbf{u}_h^n\times\Pi^0\mathbf{B}_h^n, \Pi^0\mathbf{v}_h\times\Pi^0\mathbf{B}_h^n\right)&\approx\left(\Pi^0\mathbf{u}_h^n\times\Pi^0\mathbf{B}_{h,*}^n, \Pi^0\mathbf{v}_h\times\Pi^0\mathbf{B}_h^n\right) &(99)\\
\left(\Pi^0\mathbf{u}_h^n\times\Pi^0\mathbf{B}_h^n, F_h\right)&\approx\left(\Pi^0\mathbf{u}_h^n\times\Pi^0\mathbf{B}_{h,*}^n, F_h\right), &(100)
\end{aligned}$$

and we define the linearized current density $j_{h,*}^n=\widetilde{\Pi}E_h^n+\Pi^0\mathbf{v}_h\times\Pi^0\mathbf{B}_{h,*}^n$. Since now $\mathbf{B}_h^n$ is substituted by the known field $\mathbf{B}_{h,*}^n$, the expressions on the right are bilinear forms that we can compute as matrices, yielding the following linearized scheme: *For each* $n\in[1,N]$, *find* $(\mathbf{u}_h^n, p_h^n, \mathbf{B}_h^n, E_h^n)\in\mathbf{W}_h\times Q_h\times\mathbf{V}_h^{\text{edge}}\times V_h^{\text{node}}$ *such that:*

$$\begin{aligned}
m_h(\delta_t^n\mathbf{u}_h,\mathbf{v}_h)+R_e^{-1}a_h(\mathbf{u}_h^n,\mathbf{v}_h)-b(\mathbf{v}_h,p_h^n)+s(j_{h,*}^n,\Pi^0\mathbf{v}_h\times\Pi^0\mathbf{B}_{h,*}^n)&=\left(\mathbf{f}_h^n,\mathbf{v}_h\right)\ \ \forall\mathbf{v}_h\in\mathbf{W}_{0,h}, &(101a)\\
\left[E_h^n,F_h\right]_{\text{node}}+(\Pi^0\mathbf{u}_h^n\times\Pi^0\mathbf{B}_{h,*}^n,\Pi^0F_h)-R_m^{-1}\left[\mathbf{B}_{h,*}^n,\mathbf{rot}\,F_h\right]_{\text{edge}}&=0\quad\forall F_h\in V_{0,h}^{\text{node}}, &(101b)\\
\left[\delta_t^n\mathbf{B}_h,\mathbf{C}_h\right]_{\text{edge}}+\left[\mathbf{rot}\,\mathbf{E}_h^n,\mathbf{C}_h\right]_{\text{edge}}&=0\quad\forall\mathbf{C}_h\in\mathbf{V}_h^{\text{edge}}, &(101c)\\
b(\mathbf{u}_h^n,q_h)&=0\quad\forall q_h\in Q_h. &(101d)
\end{aligned}$$

According to [25], we compute $\mathbf{B}_{h,*}^n$ for $n\geq 2$ as the linear extrapolation between two successive approximations, e.g., $\mathbf{B}_h^{n-1}$ and $\mathbf{B}_h^{n-2}$, by setting that

$$\frac{\mathbf{B}_{h,*}^n-\mathbf{B}_h^{n-1}}{\Delta t}=\frac{\mathbf{B}_h^{n-1}-\mathbf{B}_h^{n-2}}{\Delta t},$$

or, equivalently, through the formula

$$\mathbf{B}^n_{h,*} = 2\mathbf{B}^{n-1}_h - \mathbf{B}^{n-2}_h.$$

At the first timestep, i.e., $n = 1$, we guess $\mathbf{B}^1_{h,*} = \mathbf{B}_{h,0} = \mathcal{I}_{\text{edge}}(\mathbf{B}_0)$ through the initial solution $\mathbf{B}_0$. Finally, we present a proof that the approximations to the magnetic field provided by solving the linearized VEM (101) is still solenoidal. To this end, we first mention the standard argument that Faraday's law from the continuous system naturally enforces the divergence-free condition to the magnetic field. Indeed, from (5b) it holds that

$$\frac{\partial}{\partial t}\operatorname{div}\mathbf{B} = \operatorname{div}\frac{\partial}{\partial t}\mathbf{B} = -\operatorname{div}\mathbf{rot}\,E_h = 0.$$

Thus, the divergence if $\mathbf{B}$ is constant in time, and since the initial magnetic field $\mathbf{B}_0$ satisfies $\operatorname{div}\mathbf{B}_0 = 0$, then, this property is preserved throughout the evolution of the system. The following theorem states that this property also holds for the discrete magnetic field $\mathbf{B}_h$ that is solution of the linearized system (101).

Theorem 5.1. *For every time-step $n > 0$ the magnetic field satisfies*

$$\operatorname{div}\mathbf{B}^n_h = \operatorname{div}\mathbf{B}^{n-1}_h. \tag{102}$$

and the discrete magnetic field $\mathbf{B}_h$ solving (101) is solenoidal if the initial condition of the continuous problem is solenoidal, i.e., $\operatorname{div}\mathbf{B}_0 = 0$.

Proof. The proof mimics the argument mentioned above. The discrete Faraday's law (101b) implies that $\mathbf{rot}\big(V^{\text{node}}_h\big) \subset \mathbf{V}^{\text{edge}}_h$. Therefore, we obtain the time evolution equation for $\mathbf{B}^n_h$, which reads as

$$\mathbf{B}^n_h = \mathbf{B}^{n-1}_h + \Delta t\,\mathbf{rot}\,E_h. \tag{103}$$

Taking the divergence of both sides above yields the first theorem's assertion, i.e., (102). Eq. (102) implies that the divergence of the discrete magnetic field does not change in time. Then, repeating inductively Eq. (102) we need only show that $\operatorname{div}\mathbf{B}^0_h = 0$ to prove that $\mathbf{B}_h$ is a divergence-free field. To this end, we use the commuting property of the diagram in Theorem 3.3, which implies that

$$\operatorname{div}\mathbf{B}^0_h = \operatorname{div}\mathcal{I}_{\text{edge}}(\mathbf{B}_0) = \mathcal{I}_{\text{cell}}(\operatorname{div}\mathbf{B}_0) = 0, \tag{104}$$

and the second assertion of the theorem follows. □

The same argument can be used to prove that also the discrete magnetic field that solves the non-linearized VEM, i.e., system (19), is a divergence-free field.

6. Well-posedness analysis

Throughout this section, we will fix the value of $n \in \mathbb{N}$ (and remove the superscript n) and we study the well-posedness of the linearized VEM (101). To this end, we introduce two equivalent auxiliary problems and show that they are inf–sup stable saddle-point problems.

To ease the exposition, we assume homogeneous Dirichlet boundary conditions, i.e., $\mathbf{u}_b = 0$ and $E_b = 0$ on $\partial\Omega$. We consider the functional space $\mathcal{X}_h = \mathbf{W}_{0,h} \times \mathbf{V}^{\text{edge}}_h \times V^{\text{node}}_{0,h}$, endowed with the norm

$$|||\boldsymbol{\xi}_h|||^2_{\mathcal{X}_h} := |||\mathbf{u}_h|||^2_{\Delta t,\nabla} + |||\mathbf{B}_h|||^2_{\Delta t,\text{div}} + |||E_h|||^2_{\Delta t,\mathbf{rot}}, \tag{105}$$

for $\boldsymbol{\xi}_h = (\mathbf{u}_h, \mathbf{B}_h, E_h) \in \mathcal{X}_h$, where

$$|||\mathbf{u}_h|||^2_{\Delta t,\nabla} := \Delta t^{-1}|||\mathbf{u}_h|||^2_{\mathbf{W}_h} + a_h(\mathbf{u}_h,\mathbf{u}_h) + \Delta t^{-1}|||\operatorname{div}\mathbf{u}_h|||^2_{Q_h}, \tag{106a}$$

$$|||\mathbf{B}_h|||^2_{\Delta t,\text{div}} := \Delta t^{-1}|||\mathbf{B}_h|||^2_{\text{edge}} + |||\operatorname{div}\mathbf{B}_h|||^2_{\text{cell}}, \tag{106b}$$

$$|||E_h|||^2_{\Delta t,\mathbf{rot}} := |||E_h|||^2_{\text{node}} + \Delta t|||\mathbf{rot}\,E_h|||^2_{\text{edge}}. \tag{106c}$$

Then, we consider the two bilinear forms $c_h, c_{0,h} : \mathcal{X}_h \times \mathcal{X}_h \to \mathbb{R}$ given by

$$c_h(\boldsymbol{\xi}_h,\boldsymbol{\eta}_h) := \ell_1(\mathbf{v}_h) + \ell_2(F_h) + \ell_3(\mathbf{C}_h), \tag{107a}$$

$$c_{0,h}(\boldsymbol{\xi}_h,\boldsymbol{\eta}_h) := c_h(\boldsymbol{\xi}_h,\boldsymbol{\eta}_h) + \big[\operatorname{div}\mathbf{B}_h, \operatorname{div}\mathbf{C}_h\big]_{\text{cell}}, \tag{107b}$$

for $\boldsymbol{\xi}_h = (\mathbf{u}_h, \mathbf{B}_h, E_h)$ and $\boldsymbol{\eta}_h = (\mathbf{v}_h, \mathbf{C}_h, F_h)$, where

$$\ell_1(\mathbf{v}_h) = \Delta t^{-1} m_h(\mathbf{u}_h, \mathbf{v}_h) + R_e^{-1} a_h(\mathbf{u}_h, \mathbf{v}_h) + s\big(\widetilde{\Pi} E_h, \Pi^0 \mathbf{v}_h \times \Pi^0 \mathbf{B}_{h,*}^n\big) + s\big(\Pi^0 \mathbf{u}_h \times \Pi^0 \mathbf{B}_{h,*}^n, \Pi^0 \mathbf{v}_h \times \Pi^0 \mathbf{B}_{h,*}^n\big), \tag{108a}$$

$$\ell_2(F_h) = s\big[E_h, F_h\big]_{\text{node}} + s\big(\Pi^0 \mathbf{u}_h \times \Pi^0 \mathbf{B}_{h,*}^n, F_h\big) - s R_m^{-1} \big[\mathbf{B}_h, \mathbf{rot}\, F_h\big]_{\text{edge}}, \tag{108b}$$

$$\ell_3(\mathbf{C}_h) = s R_m^{-1} \big(\Delta t^{-1} \big[\mathbf{B}_h, \mathbf{C}_h\big]_{\text{edge}} + \big[\mathbf{rot}\, E_h, \mathbf{C}_h\big]_{\text{edge}}\big) \tag{108c}$$

By introducing $\ell_3^*(\mathbf{C}_h) = \ell_3(\mathbf{C}_h) + \big[\operatorname{div} \mathbf{B}_h, \operatorname{div} \mathbf{C}_h\big]_{\text{cell}}$, we can also redefine $c_{0,h}(\boldsymbol{\xi}_h, \boldsymbol{\eta}_h)$ as

$$c_{0,h}(\boldsymbol{\xi}_h, \boldsymbol{\eta}_h) = \ell_1(\mathbf{v}_h) + \ell_2(F_h) + \ell_3^*(\mathbf{C}_h). \tag{109}$$

The linearized VEM (101) is equivalent to the problem: *Find* $\boldsymbol{\xi}_h = (\hat{\mathbf{u}}_h, \mathbf{B}_h, \hat{E}_h) \in \mathcal{X}_h$ *and* $p_h \in Q_h$ *such that*

$$c_h(\boldsymbol{\xi}_h, \boldsymbol{\eta}_h) - b(\mathbf{v}_h, p_h) = \langle \mathbf{f}_h^n, \mathbf{v}_h \rangle + \Delta t^{-1} m_h(\mathbf{u}_h^{n-1}, \mathbf{v}_h) + s R_m^{-1} \Delta t^{-1} \big[\mathbf{B}_h^{n-1}, \mathbf{C}_h\big]_{\text{edge}}, \tag{110a}$$

$$b(\hat{\mathbf{u}}_h, q_h) = 0, \tag{110b}$$

for all $\boldsymbol{\eta}_h \in \mathcal{X}_h$ *and* $q_h \in Q_h$.

However, the saddle-point analysis is more naturally carried out for the following problem: *Find* $\boldsymbol{\xi}_h = (\hat{\mathbf{u}}_h, \mathbf{B}_h, \hat{E}_h) \in \mathcal{X}_h$ *and* $p_h \in Q_h$ *such that*

$$c_{0,h}(\boldsymbol{\xi}_h, \boldsymbol{\eta}_h) - b(\mathbf{v}_h, p_h) = \langle \mathbf{f}_h^n, \mathbf{v}_h \rangle + \Delta t^{-1} m_h(\mathbf{u}_h^{n-1}, \mathbf{v}_h) + s R_m^{-1} \Delta t^{-1} \big[\mathbf{B}_h^{n-1}, \mathbf{C}_h\big]_{\text{edge}}, \tag{111a}$$

$$b(\hat{\mathbf{u}}_h, q_h) = 0, \tag{111b}$$

for all $\boldsymbol{\eta}_h \in \mathcal{X}_h$ *and* $q_h \in Q_h$.

So, we first establish the equivalence between problems (110) and (111). To do this, we show that the magnetic field arising from the solution to (111) is solenoidal as stated in the following lemma.

Lemma 6.1. *Let* $\boldsymbol{\xi}_h = (\hat{\mathbf{u}}_h, \mathbf{B}_h, \hat{E}_h) \in \mathcal{X}_h$ *and* $p_h \in Q_h$ *solve* (111) *with an initial divergence-free magnetic field* $\mathbf{B}_{h,0}$, *i.e.,* $\operatorname{div} \mathbf{B}_{h,0} = 0$. *Then, the discrete magnetic field is divergence free, so it holds that* $\operatorname{div} \mathbf{B}_h = 0$,

Proof. We prove the lemma inductively. We already know that $\operatorname{div} \mathbf{B}_{h,0} = 0$ from the hypothesis; so, we are only left to prove that $\operatorname{div} \mathbf{B}_h^{n-1} = 0$ implies that $\operatorname{div} \mathbf{B}_h = 0$. To this end, we test (111) against $\boldsymbol{\eta}_h = (0, \mathbf{C}_h, 0)$ and $q_h = 0$ and we find that

$$s R_m^{-1} \Delta t^{-1} \big[\mathbf{B}_h + \Delta t \mathbf{rot}\, \hat{E}_h, \mathbf{C}_h\big]_{\text{edge}} + \big[\operatorname{div} \mathbf{B}_h, \operatorname{div} \mathbf{C}_h\big]_{\text{cell}} = s R_m^{-1} \Delta t^{-1} \big[\mathbf{B}_h^{n-1}, \mathbf{C}_h\big]_{\text{edge}},$$

or, equivalently, that

$$s R_m^{-1} \big[\Delta t^{-1} (\mathbf{B}_h - \mathbf{B}_h^{n-1}) + \mathbf{rot}\, \hat{E}_h, \mathbf{C}_h\big]_{\text{edge}} + \big[\operatorname{div} \mathbf{B}_h, \operatorname{div} \mathbf{C}_h\big]_{\text{cell}} = 0. \tag{112}$$

We set $\mathbf{C}_h = \Delta t^{-1} \left(\mathbf{B}_h - \mathbf{B}_h^{n-1}\right) + \mathbf{rot}\, \hat{E}_h$, and note that $\operatorname{div} \mathbf{C}_h = \Delta t^{-1} \operatorname{div}\big(\mathbf{B}_h - \mathbf{B}_h^{-1}\big)$ since $\operatorname{div} \mathbf{rot}\, \hat{E}_h = 0$. We substitute $\mathbf{C}_h$ in (112) and we find that

$$s R_m^{-1} \| \Delta t^{-1} (\mathbf{B}_h - \mathbf{B}_h^{n-1}) + \mathbf{rot}\, \hat{E}_h \|_{\text{edge}}^2 + \Delta t^{-1} \big[\operatorname{div} \mathbf{B}_h, \operatorname{div}(\mathbf{B}_h - \mathbf{B}_h^{n-1})\big]_{\text{cell}} = 0.$$

If $\operatorname{div} \mathbf{B}_h^{n-1} = 0$, we obtain

$$s R_m^{-1} \| \Delta t^{-1} (\mathbf{B}_h - \mathbf{B}_h^{n-1}) + \mathbf{rot}\, \hat{E}_h \|_{\text{edge}}^2 + \Delta t^{-1} \| \operatorname{div} \mathbf{B}_h \|_{\text{cell}}^2 = 0.$$

which implies that $\| \operatorname{div} \mathbf{B}_h \|_{\text{cell}} = 0$; hence, $\operatorname{div} \mathbf{B}_h = 0$. □

The result of the above theorem can be leveraged to show that both problems (110) and (111) are equivalent. We present this result in the following lemma:

Lemma 6.2. *Problems* (110) *and* (111) *are equivalent.*

Proof. If $\boldsymbol{\xi}_h = (\mathbf{u}_h, \mathbf{B}_h, \hat{E}_h) \in \mathcal{X}_h$ and $p_h \in Q_h$ solve the linear system (110), then Theorem 5.1 implies that $\operatorname{div} \mathbf{B}_h = 0$. Therefore, from (107b) we find that

$$c_{0,h}(\boldsymbol{\xi}_h, \boldsymbol{\eta}_h) = c_h(\boldsymbol{\xi}_h, \boldsymbol{\eta}_h) \qquad \forall \boldsymbol{\eta}_h \in \mathcal{X}_h, \tag{113}$$

implying that $\boldsymbol{\xi}_h$ and p_h solve (111). Conversely, if $\boldsymbol{\xi}_h = (\mathbf{u}_h, \mathbf{B}_h, \hat{E}_h)$ and p_h solve the linear system (111), then by Lemma 6.1 we know that $\operatorname{div} \mathbf{B}_h = 0$ and Eq. (113) is satisfied. Therefore, $\boldsymbol{\xi}_h$ and p_h solve (110). □

To prove that the equivalent formulation (111) is inf–sup stable, we need two technical lemmas that we state and prove below.

Lemma 6.3. *The bilinear form $c_{0,h}(\cdot,\cdot)$ is continuous in the norm defined by (105) provided that $s(\alpha^{-1}) < 1$.*

Proof. Let $\boldsymbol{\xi}_h = (\mathbf{u}_h, \mathbf{B}_h, E_h)$ and $\boldsymbol{\eta}_h = (\mathbf{v}_h, \mathbf{C}_h, F_h)$ be arbitrary elements in $\mathcal{X}_h$. A series of applications of the Cauchy–Schwartz inequality yields that

$$\Delta t^{-1} m_h(\mathbf{u}_h, \mathbf{v}_h) \le \Delta t^{-1/2} |\!|\!| \mathbf{u}_h |\!|\!|_{\mathbf{W}_h} \Delta t^{-1/2} |\!|\!| \mathbf{v}_h |\!|\!|_{\mathbf{W}_h} \le |\!|\!| \mathbf{u}_h |\!|\!|_{\Delta t,\nabla} |\!|\!| \mathbf{v}_h |\!|\!|_{\Delta t,\nabla}, \tag{114}$$

$$a_h(\mathbf{u}_h, \mathbf{v}_h) \le a_h(\mathbf{u}_h, \mathbf{u}_h)^{\frac{1}{2}} a_h(\mathbf{v}_h, \mathbf{v}_h)^{\frac{1}{2}} \le |\!|\!| \mathbf{u}_h |\!|\!|_{\Delta t,\nabla} |\!|\!| \mathbf{v}_h |\!|\!|_{\Delta t,\nabla} \tag{115}$$

$$\Delta t^{-1} \big[\mathbf{B}_h, \mathbf{C}_h\big]_{\text{edge}} \le \Delta t^{-1/2} |\!|\!| \mathbf{B}_h |\!|\!|_{\text{edge}} \Delta t^{-1/2} |\!|\!| \mathbf{C}_h |\!|\!|_{\text{edge}} \le |\!|\!| \mathbf{B}_h |\!|\!|_{\Delta t,\text{div}} |\!|\!| \mathbf{C}_h |\!|\!|_{\Delta t,\text{div}}, \tag{116}$$

$$\big[\mathbf{rot}\, E_h, \mathbf{C}_h\big]_{\text{edge}} \le \Delta t^{1/2} |\!|\!| \mathbf{rot}\, E_h |\!|\!|_{\text{edge}} \Delta t^{-1/2} |\!|\!| \mathbf{C}_h |\!|\!|_{\text{edge}} \le |\!|\!| E_h |\!|\!|_{\Delta t,\mathbf{rot}} |\!|\!| \mathbf{C}_h |\!|\!|_{\Delta t,\text{div}}, \tag{117}$$

$$\big[E_h, F_h\big]_{\text{node}} \le |\!|\!| E_h |\!|\!|_{\text{node}} |\!|\!| F_h |\!|\!|_{\text{node}} \le |\!|\!| E_h |\!|\!|_{\Delta t,\mathbf{rot}} |\!|\!| F_h |\!|\!|_{\Delta t,\mathbf{rot}}, \tag{118}$$

$$\big[\operatorname{div} \mathbf{B}_h, \operatorname{div} \mathbf{C}_h\big]_{\text{cell}} \le |\!|\!| \operatorname{div} \mathbf{B}_h |\!|\!|_{\text{cell}} |\!|\!| \operatorname{div} \mathbf{C}_h |\!|\!|_{\text{cell}} \le |\!|\!| \mathbf{B}_h |\!|\!|_{\Delta t,\text{div}}, |\!|\!| \mathbf{C}_h |\!|\!|_{\Delta t,\text{div}}. \tag{119}$$

Continuity of the coupling terms comes about by similar arguments. To derive an upper bound for the two representative terms in (108a) and (108b) we note that $\|F_h\|_{0,\Omega} \le C \|\nabla F_h\|_{0,\Omega} = \|\mathbf{rot}\, F_h\|_{0,\Omega}$ for every $F_h \in V_{0,h}^{\text{node}} \subset H_0^1(\Omega)$, where the strictly-positive constant C is independent of Δt and h. Thus, the first coupling term is bounded as follows:

$$\begin{aligned}
(\mathbf{u}_h \times \Pi^0 \mathbf{B}_{h,*}, \mathbf{v}_h \times \Pi^0 \mathbf{B}_{h,*}) &\le \|\Pi^0 \mathbf{u}_h \times \Pi^0 \mathbf{B}_{h,*}\|_{0,\Omega} \|\Pi^0 \mathbf{v}_h \times \Pi^0 \mathbf{B}_{h,*}\|_{0,\Omega} \\
&\le \|\Pi^0 \mathbf{B}_{h,*}\|_\infty^2 \|\mathbf{u}_h\|_{0,\Omega} \|\mathbf{v}_h\|_{0,\Omega} \\
&\le C \Delta t^2 \|\Pi^0 \mathbf{B}_{h,*}\|_\infty^2 \Delta t^{-1} \|\nabla \mathbf{u}_h\|_{0,\Omega} \Delta t^{-1} \|\nabla \mathbf{v}_h\|_{0,\Omega} \\
&\le C \Delta t^2 \|\Pi^0 \mathbf{B}_{h,*}\|_\infty^2 |\!|\!| \mathbf{u}_h |\!|\!|_{\Delta t,\nabla} |\!|\!| \mathbf{v}_h |\!|\!|_{\Delta t,\nabla}.
\end{aligned}$$

The second coupling term is bounded as follows:

$$\begin{aligned}
(\Pi^0 \mathbf{u}_h \times \Pi^0 \mathbf{B}_{h,*}, \widetilde{\Pi} F_h) &\le \|\Pi^0 \mathbf{u}_h \times \Pi^0 \mathbf{B}_{h,*}\|_{0,\Omega} \|\widetilde{\Pi} F_h\|_{0,\Omega} \\
&\le \|\Pi^0 \mathbf{B}_{h,*}\|_\infty \|\Pi^0 \mathbf{u}_h\|_{0,\Omega} \|\widetilde{\Pi} F_h\|_{0,\Omega} \\
&\le \|\Pi^0 \mathbf{B}_{h,*}\|_\infty \|\mathbf{u}_h\|_{0,\Omega} \|F_h\|_{0,\Omega} \\
&\le \Delta t \|\Pi^0 \mathbf{B}_{h,*}\|_\infty \Delta t^{-1} \|\mathbf{u}_h\|_{0,\Omega} \|F_h\|_{0,\Omega} \\
&\le C \|\Pi^0 \mathbf{B}_{h,*}\|_\infty |\!|\!| \mathbf{u}_h |\!|\!|_{\Delta t,\nabla} |\!|\!| F_h |\!|\!|_{\Delta t,\mathbf{rot}}.
\end{aligned}$$

The assertion of the lemma follows by noting that $\Pi^0 \mathbf{B}_{h,*} = 2\Pi^0 \mathbf{B}_h^{n-1} - \Pi^0 \mathbf{B}_h^{n-2}$ and, thus, it is bounded at any timestep since we can recursively assume that $\Pi^0 \mathbf{B}_h^{n-1}$ and $\Pi^0 \mathbf{B}_h^{n-2}$ are bounded, and using all the inequalities above to derive an upper bound for the bilinear form $|c_{0,h}(\cdot,\cdot)|$. □

Next, we prove that the bilinear form $c_{0,h}$ is inf–sup stable on the kernel of the bilinear form $b(\cdot,\cdot)$.

Lemma 6.4. *There exists a positive constant $\beta > 0$ independent of Δt and h such that*

$$\inf_{\boldsymbol{\xi}_h \in \mathcal{X}_{0,h}} \sup_{\boldsymbol{\eta}_h \in \mathcal{X}_{0,h}} \frac{c_{0,h}(\boldsymbol{\xi}_h, \boldsymbol{\eta}_h)}{|\!|\!| \boldsymbol{\xi}_h |\!|\!|_{\mathcal{X}_h} |\!|\!| \boldsymbol{\eta}_h |\!|\!|_{\mathcal{X}_h}} \ge \beta, \tag{120}$$

where $\mathcal{X}_{0,h} = \big\{(\mathbf{v}_h, \mathbf{B}_h, E_h) \in \mathcal{X}_h$ such that $\operatorname{div} \mathbf{v}_h = 0\big\}$.

Proof. To prove the lemma statement, we will prove that for every virtual element field $\boldsymbol{\xi}_h \in \mathcal{X}_h$, there exists a virtual element field $\boldsymbol{\eta}_h \in \mathcal{X}_h$ such that

$$|\!|\!| \boldsymbol{\xi}_h |\!|\!|_{\mathcal{X}_h} \ge \beta_1 |\!|\!| \boldsymbol{\eta}_h |\!|\!|_{\mathcal{X}_h} \quad \text{and} \quad c_{0,h}(\boldsymbol{\xi}_h, \boldsymbol{\eta}_h) \ge \beta_2 |\!|\!| \boldsymbol{\xi}_h |\!|\!|_{\mathcal{X}_h}^2 \tag{121}$$

for some pair of positive constants β_1 and β_2, which are independent of h and Δt. Relations (121) imply (120) by assuming $\beta = \beta_1\beta_2$.

For any $\boldsymbol{\xi}_h = (\mathbf{u}_h, \mathbf{B}_h, E_h)$, we obtain a virtual element field $\boldsymbol{\eta}_h = (\mathbf{v}_h, \mathbf{C}_h, F_h)$ satisfying inequalities (121) by setting

$$\mathbf{v}_h = \mathbf{u}_h, \quad \mathbf{C}_h = \frac{1}{2}(\mathbf{B}_h + \Delta t \mathbf{rot}\, E_h), \quad F_h = E_h. \tag{122}$$

Indeed, from the definition of $|||\cdot|||_{\Delta t,\mathrm{div}}$, cf. (106b), and an application of the triangular inequality, we find that

$$\begin{aligned}
|||\mathbf{B}_h + \Delta t \mathbf{rot}\, E_h|||^2_{\Delta t,\mathrm{div}} &= \Delta t^{-1}|||\mathbf{B}_h + \Delta t \mathbf{rot}\, E_h|||^2_{\mathrm{edge}} + |||\mathrm{div}\, \mathbf{B}_h|||^2_{\mathrm{cell}} \\
&\le 2\Delta t^{-1}|||\mathbf{B}_h|||^2_{\mathrm{edge}} + 2\Delta t|||\mathbf{rot}\, E_h|||^2_{\mathrm{edge}} + |||\mathrm{div}\, \mathbf{B}_h|||^2_{\mathrm{cell}} \\
&= 2|||\mathbf{B}_h|||^2_{\Delta t,\mathrm{div}} + 2\Delta t|||\mathbf{rot}\, E_h|||^2_{\mathrm{edge}}.
\end{aligned} \tag{123}$$

Then, we use (123) in the definition of $|||\boldsymbol{\eta}_h|||^2_{\mathcal{X}_h}$, cf. (105), and we obtain

$$\begin{aligned}
|||\boldsymbol{\eta}_h|||^2_{\mathcal{X}_h} &= |||\mathbf{u}_h|||^2_{\Delta t,\nabla} + \frac{1}{4}|||\mathbf{B}_h + \Delta t \mathbf{rot}\, E_h|||^2_{\Delta t,\mathrm{div}} + |||E_h|||^2_{\Delta t,\mathbf{rot}} \\
&\le |||\mathbf{u}_h|||^2_{\Delta t,\nabla} + \frac{1}{2}|||\mathbf{B}_h|||^2_{\Delta t,\mathrm{div}} + \frac{1}{2}\Delta t|||\mathbf{rot}\, E_h|||^2_{\mathrm{edge}} + |||E_h|||^2_{\Delta t,\mathbf{rot}} \\
&\le |||\mathbf{u}_h|||^2_{\Delta t,\nabla} + \frac{1}{2}|||\mathbf{B}_h|||^2_{\Delta t,\mathrm{div}} + \frac{3}{2}|||E_h|||^2_{\Delta t,\mathbf{rot}} \le \frac{3}{2}|||\boldsymbol{\xi}_h|||^2_{\mathcal{X}_h}.
\end{aligned} \tag{124}$$

The inequality chain (124) implies the first inequality of (121) by setting $\beta_1 = \sqrt{2/3}$.

To prove the second inequality of (121), we first note that

$$\begin{aligned}
\ell_1(\mathbf{u}_h) &= \Delta t^{-1}|||\mathbf{u}_h|||^2_{\mathbf{W}_h} + R_e^{-1}a_h(\mathbf{u}_h, \mathbf{u}_h) + s(\widetilde{\Pi}E_h, \Pi^0\mathbf{u}_h \times \Pi^0\mathbf{B}^n_{h,*}) \\
&\qquad + s(\Pi^0\mathbf{u}_h \times \Pi^0\mathbf{B}^n_{h,*}, \Pi^0\mathbf{u}_h \times \Pi^0\mathbf{B}^n_{h,*}).
\end{aligned} \tag{125a}$$

$$\ell_2(E_h) = s|||E_h|||^2_{\mathrm{node}} + s(\Pi^0\mathbf{u}_h \times \Pi^0\mathbf{B}^n_{h,*}, \widetilde{\Pi}E_h) - sR_m^{-1}\big[\mathbf{B}_h, \mathbf{rot}\, E_h\big]_{\mathrm{edge}} \tag{125b}$$

$$\begin{aligned}
\ell_3^*\big((\mathbf{B}_h + \Delta t \mathbf{rot}\, E_h)/2\big) &= \frac{sR_m^{-1}}{2}\big(\Delta t^{-1}|||\mathbf{B}_h|||^2_{\mathrm{edge}} + 2[\mathbf{rot}\, E_h, \mathbf{B}_h]_{\mathrm{edge}} \\
&\qquad + \Delta t|||\mathbf{rot}\, E_h|||^2_{\mathrm{edge}} + |||\mathrm{div}\, \mathbf{B}_h|||^2_{\mathrm{cell}}\big),
\end{aligned} \tag{125c}$$

where we recall that $\ell_3^*(\cdot)$ was introduced in (109).

Then, using the definition of the nodal norm based on the inner product (42) and noting that the stabilization term $\mathcal{S}^V(\cdot,\cdot)$ is nonnegative, we obtain the estimate

$$\begin{aligned}
&|||E_h|||^2_{\mathrm{node}} + (\widetilde{\Pi}E_h, \Pi^0\mathbf{u}_h \times \Pi^0\mathbf{B}^n_{h,*}) + (\Pi^0\mathbf{u}_h \times \Pi^0\mathbf{B}^n_{h,*}, \Pi^0\mathbf{u}_h \times \Pi^0\mathbf{B}^n_{h,*}) \\
&\qquad + (\Pi^0\mathbf{u}_h \times \Pi^0\mathbf{B}^n_{h,*}, \widetilde{\Pi}E_h) \\
&= \big(\widetilde{\Pi}E_h, \widetilde{\Pi}E_h\big) + \mathcal{S}^V\big((\mathcal{I} - \widetilde{\Pi})E_h, (\mathcal{I} - \widetilde{\Pi})E_h\big) + 2(\widetilde{\Pi}E_h, \Pi^0\mathbf{u}_h \times \Pi^0\mathbf{B}^n_{h,*}) \\
&\qquad + (\Pi^0\mathbf{u}_h \times \Pi^0\mathbf{B}^n_{h,*}, \Pi^0\mathbf{u}_h \times \Pi^0\mathbf{B}^n_{h,*}) \\
&\ge \big(\widetilde{\Pi}E_h, \widetilde{\Pi}E_h\big) + 2\big(\widetilde{\Pi}E_h, \Pi^0\mathbf{u}_h \times \Pi^0\mathbf{B}^n_{h,*}\big) + \big(\Pi^0\mathbf{u}_h \times \Pi^0\mathbf{B}^n_{h,*}, \Pi^0\mathbf{u}_h \times \Pi^0\mathbf{B}^n_{h,*}\big) \\
&= \big(\widetilde{\Pi}E_h + \Pi^0\mathbf{u}_h \times \Pi^0\mathbf{B}^n_{h,*}, \widetilde{\Pi}E_h + \Pi^0\mathbf{u}_h \times \Pi^0\mathbf{B}^n_{h,*}\big) \\
&= \|\widetilde{\Pi}E_h + \Pi^0\mathbf{u}_h \times \Pi^0\mathbf{B}^n_{h,*}\|^2_{0,\Omega}.
\end{aligned} \tag{126}$$

Next, we add Eqs. (125a), (125b), and (125c) together, and use the positive term resulting from (126) to obtain:

$$\begin{aligned}
c_{0,h}(\boldsymbol{\xi}_h, \boldsymbol{\eta}_h) &= \ell_1(\mathbf{u}_h) + \ell_2(E_h) + \ell_3^*\big((\mathbf{B}_h + \Delta t \mathbf{rot}\, E_h)/2\big) \\
&\ge \Delta t^{-1}|||\mathbf{u}_h|||^2_{\mathbf{W}_h} + R_e^{-1}a_h(\mathbf{u}_h, \mathbf{u}_h) + s\|\widetilde{\Pi}E_h + \Pi^0\mathbf{u}_h \times \Pi^0\mathbf{B}^n_{h,*}\|^2_{0,\Omega}. \\
&\quad - sR_m^{-1}\big[\mathbf{B}_h, \mathbf{rot}\, E_h\big]_{\mathrm{edge}} + \frac{sR_m^{-1}}{2}\Delta t^{-1}|||\mathbf{B}_h|||^2_{\mathrm{edge}} \\
&\quad + sR_m^{-1}\big[\mathbf{rot}\, E_h, \mathbf{B}_h\big]_{\mathrm{edge}} + sR_m^{-1}\Delta t|||\mathbf{rot}\, E_h|||^2_{\mathrm{edge}} \\
&\quad + sR_m^{-1}|||\mathrm{div}\, \mathbf{B}_h|||^2_{\mathrm{cell}}.
\end{aligned} \tag{127}$$

We note that:

$$\begin{aligned}\|E_h\|^2_{0,\Omega} &\leq 2\|\widetilde{\Pi}E_h + \Pi^0\mathbf{u}_h \times \Pi^0\mathbf{B}^n_{h,*}\|^2_{0,\Omega} + 2\|\Pi^0\mathbf{u}_h \times \Pi^0\mathbf{B}^n_{h,*}\|^2_{0,\Omega}\\ &\leq 2\|\widetilde{\Pi}E_h + \Pi^0\mathbf{u}_h \times \Pi^0\mathbf{B}^n_{h,*}\|^2_{0,\Omega} + 2\|\Pi^0\mathbf{B}^n_{h,*}\|^2_{\infty,\Omega}2\,\|\Pi^0\mathbf{u}_h\|^2_{0,\Omega}\\ &\leq 2\max\big(1,\,\|\Pi^0\mathbf{B}^n_{h,*}\|^2_{\infty,\Omega}\big)\big(\|\widetilde{\Pi}E_h + \Pi^0\mathbf{u}_h \times \Pi^0\mathbf{B}^n_{h,*}\|^2_{0,\Omega} + \|\mathbf{u}_h\|^2_{0,\Omega}\big)\\ &\leq 2\max\big(1,\,\|\Pi^0\mathbf{B}^n_{h,*}\|^2_{\infty,\Omega}\big)\max\left(1,\frac{2}{\mu_*}\right)\Big(\|\widetilde{\Pi}E_h + \Pi^0\mathbf{u}_h \times \Pi^0\mathbf{B}^n_{h,*}\|^2_{0,\Omega} + \frac{\mu_*}{2}\|\mathbf{u}_h\|^2_{0,\Omega}\Big).\end{aligned}$$

Let $\hat{C}^{-1} = 2\max\big(1,\,\|\Pi^0\mathbf{B}^n_{h,*}\|^2_{\infty,\Omega}\big)\max\left(1,\,\frac{2}{\mu_*}\right)$. Reversing the inequality above and using the left inequality in (28) yields

$$\begin{aligned}&\Delta t^{-1}|||\mathbf{u}_h|||^2_{\mathbf{W}_h} + \|\widetilde{\Pi}E_h + \Pi^0\mathbf{u}_h \times \Pi^0\mathbf{B}^n_{h,*}\|^2_{0,\Omega}\\ &\quad\geq \frac{1}{2}\Delta t^{-1}|||\mathbf{u}_h|||^2_{\mathbf{W}_h} + \frac{\mu_*}{2}\|\mathbf{u}_h\|^2_{0,\Omega} + \|\widetilde{\Pi}E_h + \Pi^0\mathbf{u}_h \times \Pi^0\mathbf{B}^n_{h,*}\|^2_{0,\Omega}\\ &\quad\geq \frac{1}{2}\Delta t^{-1}|||\mathbf{u}_h|||^2_{\mathbf{W}_h} + \hat{C}\|E_h\|^2_{0,\Omega}\\ &\quad\geq \min\left(\frac{1}{2},\hat{C}\right)\Big(\Delta t^{-1}|||\mathbf{u}_h|||^2_{\mathbf{W}_h} + \|E_h\|^2_{0,\Omega}\Big).\end{aligned}$$

We use this inequality in (127), simplify the terms involving $\big[\mathbf{rot}\,E_h, \mathbf{B}_h\big]_{\text{edge}}$, add $|||\operatorname{div}\mathbf{u}_h|||^2_{\mathbf{W}_h} = 0$, and find that

$$\begin{aligned}c_{0,h}(\boldsymbol{\xi}_h,\boldsymbol{\eta}_h) &\geq \beta_2\Bigg(\Big[\Delta t^{-1}|||\mathbf{u}_h|||^2_{\mathbf{W}_h} + R_e^{-1}a_h(\mathbf{u}_h,\mathbf{u}_h) + |||\operatorname{div}\mathbf{u}_h|||^2_{\mathbf{W}_h}\Big]\\ &\qquad + \Big[\Delta t^{-1}|||\mathbf{B}_h|||^2_{\text{edge}} + |||\operatorname{div}\mathbf{B}_h|||^2_{\text{cell}}\Big] + \Big[|||E_h|||^2_{\text{node}} + \Delta t|||\mathbf{rot}\,E_h|||^2_{\text{edge}}\Big]\Bigg)\\ &= \beta_2\big(|||\mathbf{u}_h|||^2_{\Delta t,\nabla} + |||\mathbf{B}_h|||^2_{\Delta t,\operatorname{div}} + |||E_h|||^2_{\Delta t,\mathbf{rot}}\big) = \beta_2|||\boldsymbol{\xi}_h|||^2_{\mathcal{X}_h},\end{aligned} \tag{128}$$

with $\beta_2 = \min\big(1/2, s\hat{C}, R_e^{-1}, s/2, sR_m^{-1}/2\big)$, and using the norm definitions (105) and (106). □

Finally, we present the main result of this section.

Theorem 6.5. *The linear problem in (101) is well-posed.*

Proof. Lemmas 6.3, 6.4 Theorem 3.1 prove that the hypothesis of LBB Theorem are satisfied yielding as a conclusion that (111) is well-posed. By Lemma 6.2 problems (110) and (111) are equivalent. The well-posedness of one implies the well-posedness of both. □

We note that this well-posedness result exposes the saddle-point nature of the linear system. This result can be leveraged to come up with efficient preconditioner following the framework laid out in [30]. This was done for a similar MHD system in [31] using a Picard fixed point iteration as the choice of linearization. Efficient implementation of this preconditioner will require a generalization of mass lumping. While it is unclear how this can be done in general, in [36] some strategies are laid out in the context of elastodynamics. We also note that these type of preconditioners have been used in 3D VEMs for problems in fluid flow as well as electromagnetics, see [21]. Other physics-based preconditioners have been developed, see [19,20].

7. Numerical results

In this section we will present the results of a series of numerical experiments that shed some light on the performance of the VEM developed and analyzed throughout this article. It is divided in three subsections: the first one, Section 7.1, explores the rate of convergence; the second one, Section 7.2, relates to the preservation of

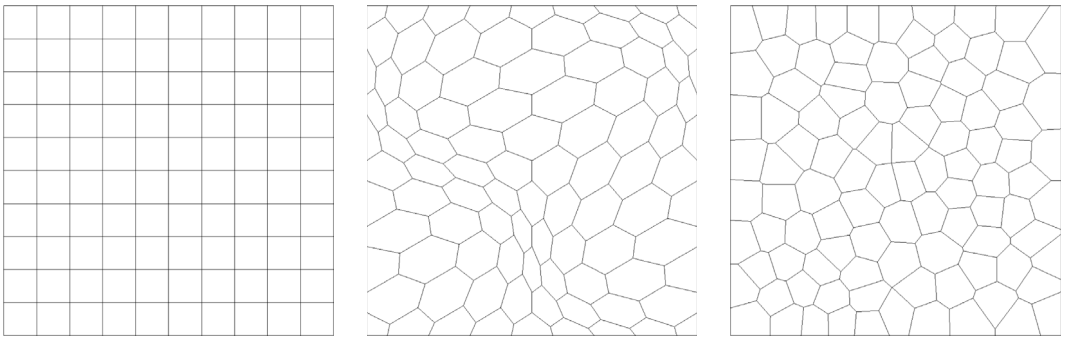

Fig. 2. Test meshes used in the convergence test. The cells of the left-most mesh are perfect squares, the cells of the mesh in the center are distorted hexagons and the right-most mesh is a Voronoi tessellation.

the divergence-free condition on the magnetic field; the last one, Section 7.3, presents the qualitative results of the classical driven-cavity problem.

7.1. Convergence test

To assess, experimentally, the rate of convergence of our method we will study approximations made on the computational domain $\Omega = [0, 1]^2$. We begin by setting the source functions, initial and boundary conditions in accordance to the exact solution:

$$\mathbf{u} = \begin{pmatrix} \cos(y+t) \\ 0 \end{pmatrix}, \quad p = \frac{1}{2}\sin 1 - x\cos y, \quad \mathbf{B} = \begin{pmatrix} 0 \\ \cos(x+t) \end{pmatrix}, \quad E = \cos(x+t). \tag{129}$$

We evolve the system until $T = 0.2$ and set the time-step parameter according to

$$\Delta t = 0.1h^2 \tag{130}$$

Our tests involve the three different mesh families illustrated in Fig. 2. We consider a family of square meshes (left panel) for comparison; a family of smoothly-remapped polygons that may have distorted elements (central panel); a family of Voronoi tessellations that can be affected by small edges. We will use four meshes of each type differing in mesh size to show that as this parameter shrinks our numerical approximations approach the manufactured solution (129). The results are summarized in Fig. 3. There we find evidence to conclude that our method achieves an optimal convergence rate. This is to say that the pressure and electric field converge quadratically in the L^2-norm, the velocity field converges quadratically in the H^1-norm and the magnetic field converges linearly in the L^2-norm.

Another conclusion that we can draw from Fig. 3 has to do with the robustness of the method. Note that, on each plot, the three convergence lines are very close to each other. This implies that regardless of the type of mesh used in our simulations, we can expect the same error. Thus, the VEM we developed is not sensitive to mesh-type.

7.2. The divergence-free condition on the magnetic field

We also tested to guarantee that the method does preserve the solenoidal nature of the magnetic field at the discrete level. We can compute the piece-wise constant divergence over each cell K using the formula:

$$\operatorname{div}\mathbf{B}_h = \frac{1}{|K|}\sum_{e\in K}\int_e \mathbf{B}_h \cdot \mathbf{n}\, \mathrm{d}\ell. \tag{131}$$

Since the quantities required can be obtained from the degrees of freedom. The initial and boundary conditions are the same as those given in Section 7.1. The results up to $T = 1$ are summarized in Table 1 and confirm the divergence-free property in this time integration domain.

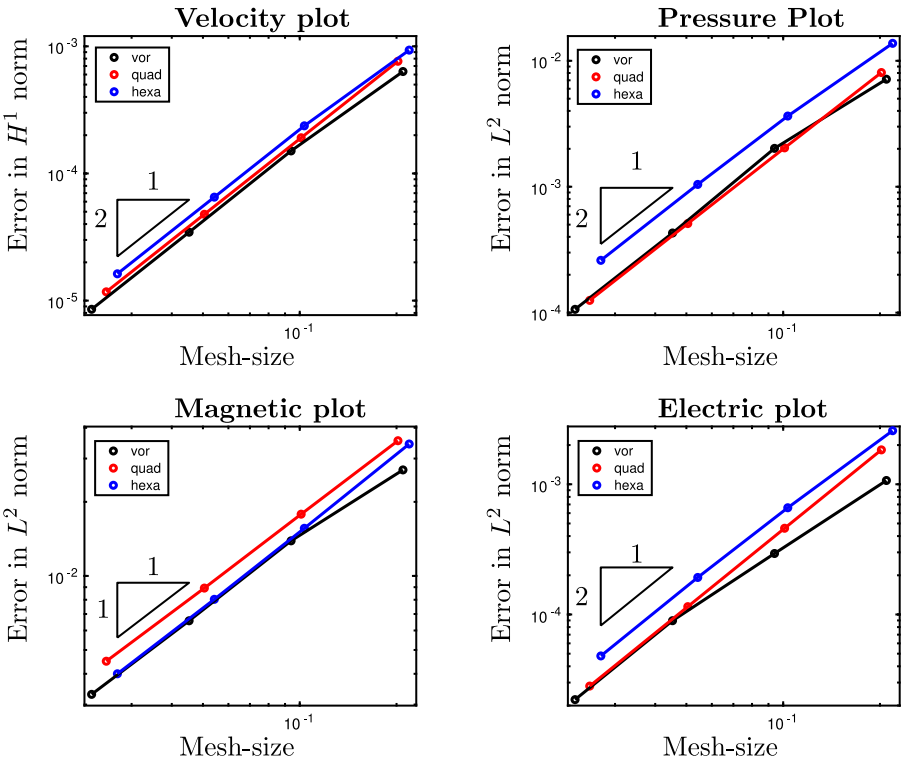

Fig. 3. Error plots for the approximation to the velocity field, pressure, magnetic field and electric fields. The three different colored lines represent the results attained in the different meshes. (For interpretation of the references to color in this figure legend, the reader is referred to the web version of this article.)

Table 1
Summary of the evolution of the square L^2 norm of the divergence of the magnetic field on the three different types of meshes.

Time	$\|\operatorname{div}\mathbf{B}_h\|_{0,\Omega}$ on a square mesh	$\|\operatorname{div}\mathbf{B}_h\|_{0,\Omega}$ on a hexagonal mesh	$\|\operatorname{div}\mathbf{B}_h\|_{0,\Omega}$ on a Voronoi tessellation
0.00	4.234e−16	3.987e−15	4.220e−15
0.25	1.640e−13	3.716e−13	5.573e−13
0.50	2.896e−13	6.485e−13	9.958e−13
0.75	3.735e−13	8.338e−13	1.313e−12
1.00	4.169e−13	9.378e−13	1.514e−12

7.3. The driven cavity test

The driven cavity problem is a classic benchmark from computational fluid mechanics. In this experiment we consider an electrically conducting fluid that is entirely trapped inside a container with hard walls. The container, in our simulations, will be the square $\Omega = [0, 1]^2$. This fluid is subjected to an external magnetic field given by the initial conditions

$$\mathbf{B}_0(x, y) = (1, 0). \tag{132}$$

We borrow the set up from [25]. The source term in the momentum equation is neglected, i.e., $\mathbf{f} \equiv 0$. The initial and boundary conditions on the velocity field are given by

$$\mathbf{u}_0(x, y) = \mathbf{u}_b(x, y, t) = (v(x, y), 0) \tag{133}$$

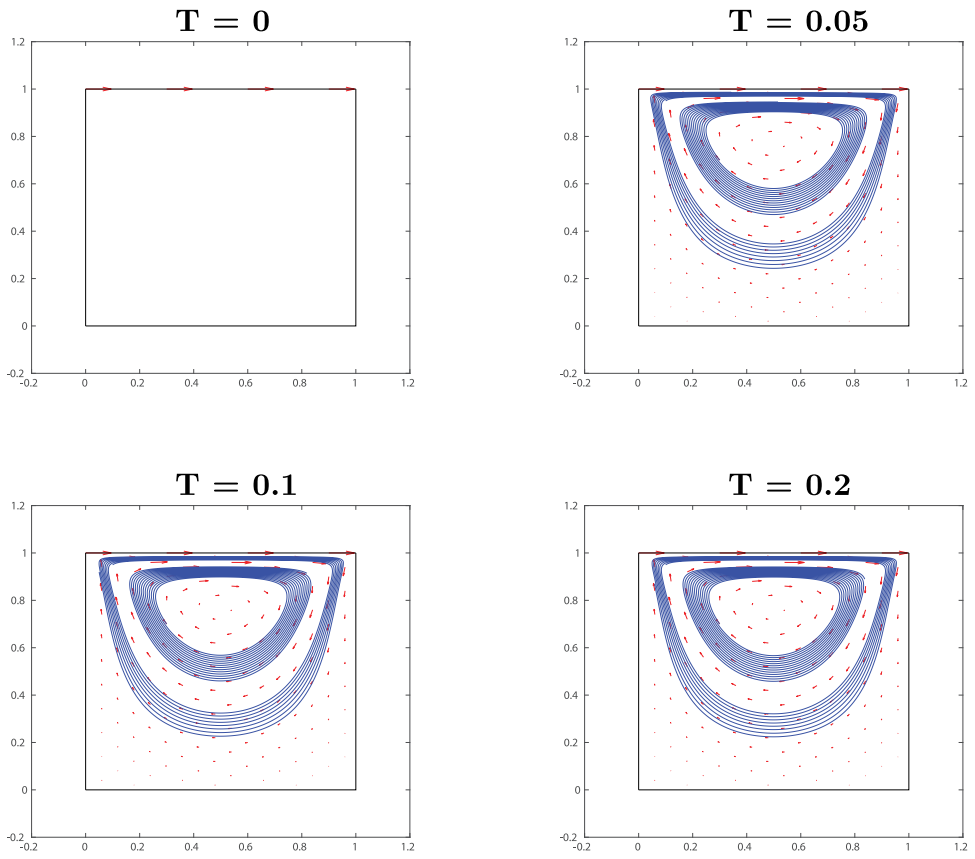

Fig. 4. Streamlines of the velocity field for the driven-cavity test at different times starting with zero velocity at time $T = 0$.

where $v \in C^1(\Omega)$ is defined as

$$v(x, y) = \begin{cases} 1 & y = 1, \\ 0 & 0 \leq y \leq 1 - h, \end{cases} \tag{134}$$

where $0 < h < 1$ is the mesh-size. Finally, we will consider the walls of our cavity to be made from a perfect conductor. This is reflected in the boundary conditions on the electric field

$$E_b(x, y, t) = 0 \tag{135}$$

One way to interpret the test is to consider a stream of some fluid with magnetic properties running in a perfectly laminar flow that flows left to right. Further consider a square cavity on its side (bottom) filled with the same fluid initially perfectly still. Thus the initial velocity field of the fluid inside the cavity is zero everywhere except for at the very top. The boundary conditions are also a consequence of the previously described stream. This influence alone will result in the fluid inside the cavity to run against the solid walls of the cavity forcing the fluid to bounce around at swirl. Thus, the result of the cavity test is that the streamlines of the velocity field will swirl around in a vortex as presented in Fig. 4.

8. Conclusions

This paper presented a VEM design for a two-dimensional incompressible MHD model coupling electromagnetics and fluid flow. The numerical method uses a set of projectors onto polynomial spaces that we can compute using only the degrees of freedom of the solution approximations, thus avoiding computing them pointwise. The continuous model involves several non-linearities. To treat them, we propose a linearization that stems from a

linear extrapolation of the magnetic field as suggested in [25] for a FEM. The main advantage of this approach is that we need to solve only one linear system at each time step. We proved that this method is well-posed by studying each linear system. Precisely, we identified each system as a saddle-point problem, and the well-posedness of the VEM follows from the more general BBL theory. The well-posedness guarantees a degree of stability in our computations. Importantly, it may serve as a basis to design efficient preconditioners, one of the topics of our future research in this field, as an application of the theory presented in [30]. It is worth mentioning that the development of such preconditioners has already been successful in the case of MHD systems for a different linearization strategy, see [31]. Finally, we presented numerical experiments that demonstrate the performance of this VEM, including testing the convergence rate, the preservation of the divergence-free condition on the magnetic field, and qualitative results of the classical driven-cavity problem.

Acknowledgments

Dr. S. Naranjo-Alvarez's work was fully supported by the italian PRIN 2017 Grant "Virtual Element Methods: Analysis and Applications" from April 2021 to February 2022 for his post-doctoral studies at the Department of Mathematics and Applications of the University of Milano-Bicocca, Italy, and during his doctoral studies by (i) the National Science Foundation (NSF), USA grant #1545188, "*NRT-DESE: Risk and uncertainty quantification in marine science and policy*", which provided a one year fellowship and internship support at Los Alamos National Laboratory (LANL), USA; (ii) the DOE-ASCR AM (Applied Math), USA base program grant for a summer internship at LANL; (iii) the graduate research funding from Prof. V. A. Bokil's DMS, USA grant #1720116 and # 2012882, an INTERN supplemental award to Professor Bokil's DMS grant # 1720116 for a second internship at LANL, and teaching support from the Department of Mathematics at Oregon State University, USA. Prof. L. Beirao da Veiga was partially supported by the italian PRIN 2017 Grant "Virtual Element Methods: Analysis and Applications". Prof. V. A. Bokil was partially supported by The National Science Foundation, USA funding from the DMS grants # 1720116 and # 2012882. Dr. V. Gyrya and Dr. G. Manzini were supported by the LDRD-ER program at LANL, USA under project number 20180428ER. Los Alamos National Laboratory is operated by Triad National Security, LLC, for the National Nuclear Security Administration of U.S. Department of Energy (Contract No. 89233218CNA000001).

References

[1] R.A. Adams, J.J.F. Fournier, Sobolev Spaces, Vol. 140, Academic Press, 2003.
[2] B. Ahmad, A. Alsaedi, F. Brezzi, L.D. Marini, A. Russo, Equivalent projectors for virtual element methods, Comput. Math. Appl. 66 (3) (2013) 376–391.
[3] P.F. Antonietti, G. Manzini, I. Mazzieri, H.M. Mourad, M. Verani, The arbitrary-order virtual element method for linear elastodynamics models. Convergence, stability and dispersion-dissipation analysis, Internat. J. Numer. Methods Engrg. 122 (4) (2021a) 934–971, http://dx.doi.org/10.1002/nme.6569.
[4] P.F. Antonietti, G. Manzini, S. Scacchi, M. Verani, A review on arbitrarily regular conforming virtual element methods for second- and higher-order elliptic partial differential equations, Math. Models Methods Appl. Sci. 31 (14) (2021b) 2825–2853, http://dx.doi.org/10.1142/S0218202521500627.
[5] P.F. Antonietti, G. Manzini, M. Verani, The conforming virtual element method for polyharmonic problems, Comput. Math. Appl. 79 (7) (2020) 2021–2034, http://dx.doi.org/10.1016/j.camwa.2019.09.022, published online: 4 October 2019.
[6] F. Armero, J.C. Simo, Long-term dissipativity of time-stepping algorithms for an abstract evolution equation with applications to the incompressible MHD and Navier-Stokes equations, Comput. Methods Appl. Mech. Engrg. 131 (1–2) (1996) 41–90.
[7] L. Beirão da Veiga, C. Lovadina, G. Vacca, Divergence free virtual elements for the Stokes problem on polygonal meshes, ESAIM Math. Model. Numer. Anal. 51 (2) (2017) 509–535.
[8] L. Beirão da Veiga, C. Lovadina, G. Vacca, Virtual elements for the Navier–Stokes problem on polygonal meshes, SIAM J. Numer. Anal. 56 (3) (2018) 1210–1242.
[9] L. Beirõ da Veiga, F. Dassi, G. Manzini, L. Mascotto, Virtual elements for maxwell's equations, Comput. Math. Appl. (2021) http://dx.doi.org/10.1016/j.camwa.2021.08.019.
[10] L. Beirão Da Veiga, F. Brezzi, L.D. Marini, A. Russo, H(div) and h(curl)-conforming virtual element methods, Numer. Math. 133 (2) (2016) 303–332.
[11] E. Benvenuti, A. Chiozzi, G. Manzini, N. Sukumar, Extended virtual element method for the Laplace problem with singularities and discontinuities, Comput. Methods Appl. Mech. Engrg. 356 (2019) 571–597, http://dx.doi.org/10.1016/j.cma.2019.07.028.
[12] Benvenuti, A. Chiozzi, G. Manzini, N. Sukumar, Extended virtual element method for two-dimensional linear elastic fracture, Comput. Methods Appl. Mech. Engrg. 390 (2022) 114352, http://dx.doi.org/10.1016/j.cma.2021.114352.
[13] S. Berrone, A. Borio, Manzini, SUPG stabilization for the nonconforming virtual element method for advection-diffusion-reaction equations, Comput. Methods Appl. Mech. Engrg. 340 (2018) 500–529.

[14] J.U. Brackbill, D.C. Barnes, The effect of nonzero Div B on the numerical solution of the magnetohydrodynamic equations, J. Comput. Phys. 35 (3) (1980) 426–430.
[15] S.C. Brenner, L.Y. Sung, Virtual element methods on meshes with small edges or faces, Math. Models Methods Appl. Sci. 28 (07) (2018) 1291–1336, http://dx.doi.org/10.1142/S0218202518500355.
[16] F. Brezzi, A. Buffa, G. Manzini, Mimetic scalar products for discrete differential forms, J. Comput. Phys. 257-Part B (2014) 1228–1259.
[17] O. Certik, F. Gardini, G. Manzini, L. Mascotto, G. Vacca, The p- and hp-versions of the virtual element method for elliptic eigenvalue problems, Comput. Math. Appl. 79 (7) (2020) 2035–2056.
[18] O. Certik, F. Gardini, G. Manzini, G. Vacca, The virtual element method for eigenvalue problems with potential terms on polytopic meshes, Appl. Math. 63 (3) (2018) 333–365.
[19] L. Chacón, An optimal, parallel, fully implicit Newton–Krylov solver for three-dimensional viscoresistive magnetohydrodynamics, Phys. Plasmas 15 (5) (2008) 056103.
[20] E.C. Cyr, J.N. Shadid, R.S. Tuminaro, R.P. Pawlowski, L. Chacón, A new approximate block factorization preconditioner for two-dimensional incompressible (reduced) resistive MHD, SIAM, J. Sci. Comput. 35 (3) (2013) B701–B730.
[21] F. Dassi, S. Scacchi, Parallel block preconditioners for three-dimensional virtual element discretizations of saddle-point problems, Comput. Methods Appl. Mech. Engrg. 372 (2020) 113424.
[22] P.A. Davidson, An introduction to magnetohydrodynamics, 2002.
[23] E. Emmrich, Discrete Versions of Gronwall's Lemma and their Application To the Numerical Analysis of Parabolic Problems, Techn. Univ., 1999.
[24] F. Gardini, G. Manzini, G. Vacca, The nonconforming virtual element method for eigenvalue problems, ESAIM Math. Model. Numer. Anal. 53 (2019) 749–774.
[25] R. Hiptmair, L. Li, S. Mao, W. Zheng, A fully divergence-free finite element method for magnetohydrodynamic equations, Math. Models Methods Appl. Sci. 28 (04) (2018) 659–695.
[26] K. Hu, Y. Ma, J. Xu, Stable finite element methods preserving div B=0 exactly for MHD models, Numer. Math. 135 (2) (2017) 371–396.
[27] K. Lipnikov, G. Manzini, F. Brezzi, A. Buffa, The mimetic finite difference method for 3D magnetostatics fields problems, J. Comput. Phys. 230 (2) (2011) 305–328, http://dx.doi.org/10.1016/j.jcp.2010.09.007.
[28] J.G. Liu, W.C. Wang, An energy-preserving MAC–yee scheme for the incompressible MHD equation, J. Comput. Phys. 174 (1) (2001) 12–37.
[29] J.G. Liu, W.C. Wang, Energy and helicity preserving schemes for hydro-and magnetohydro-dynamics flows with symmetry, J. Comput. Phys. 200 (1) (2004) 8–33.
[30] D. Loghin, A.J. Wathen, Analysis of preconditioners for saddle-point problems, SIAM J. Sci. Comput. 25 (6) (2004) 2029–2049.
[31] Y. Ma, K. Hu, X. Hu, J. Xu, Robust preconditioners for incompressible MHD models, J. Comput. Phys. 316 (2016) 721–746.
[32] P. Monk, Finite Element Methods for Maxwell's Equations, Oxford University Press, 2003.
[33] R.J. Moreau, Magnetohydrodynamics, Vol. 3, Springer Science & Business Media, 2013.
[34] J.R. Munkres, Analysis on Manifolds, CRC Press, 2018.
[35] S. Naranjo-Alvarez, A.V. Bokil, V. Gyrya, G. Manzini, The virtual element method for resistive magnetohydrodynamics, Comput. Methods Appl. Mech. Engrg. 381 (2021) 113815.
[36] K. Park, H. Chi, G.H. Paulino, On nonconvex meshes for elastodynamics using virtual element methods with explicit time integration, Comput. Methods Appl. Mech. Engrg. 356 (2019) 669–684.
[37] T. Sorgente, S. Biasotti, G. Manzini, M. Spagnuolo, The role of mesh quality and mesh quality indicators in the virtual element method, Adv. Comput. Math. 48 (3) (2022).
[38] G. Vacca, An H^1-conforming virtual element for Darcy and brinkman equations, Math. Models Methods Appl. Sci. 28 (01) (2018) 159–194.
[39] L. Beirão da Veiga, F. Brezzi, F. Dassi, L.D. Marini, A. Russo, Virtual element approximation of 2D magnetostatic problems, Comput. Methods Appl. Mech. Engrg. 327 (2017a) 173–195.
[40] L. Beirão da Veiga, F. Brezzi, F. Dassi, L.D. Marini, A. Russo, A family of three-dimensional virtual elements with applications to magnetostatics, SIAM J. Numer. Anal. 56 (5) (2018) 2940–2962.
[41] L. Beirao da Veiga, F. Brezzi, L.D. Marini, A. Russo, Mixed virtual element methods for general second order elliptic problems on polygonal meshes, ESAIM Math. Model. Numer. Anal. 50 (3) (2016) 727–747.
[42] L. Beirão da Veiga, K. Lipnikov, G. Manzini, The Mimetic Finite Difference Method for Elliptic Problems, Vol. 11, Springer, 2014.
[43] L. Beirão da Veiga, C. Lovadina, A. Russo, Stability analysis for the virtual element method, Math. Models Methods Appl. Sci. 27 (13) (2017b) 2557–2594, http://dx.doi.org/10.1142/S021820251750052X.
[44] L. Beirão da Veiga, G. Manzini, L. Mascotto, A posteriori error estimation and adaptivity in hp virtual elements, Numer. Math. 143 (2019) 139–175, http://dx.doi.org/10.1007/s00211-019-01054-6.
[45] Y. Zhang, Y. Hou, L. Shan, Numerical analysis of the Crank–Nicolson extrapolation time discrete scheme for magnetohydrodynamics flows, Numer. Methods Partial Differential Equations 31 (6) (2015) 2169–2208.